Table of Contents - Issue 31, 2012

Full papers:

Metal–Fluorocarbon Pyrolants. XV: Combustion of two Ytterbium–Halocarbon Formulations 3

Ernst-Christian Koch,Volker Weiser, Evelin Roth, Sebastian Knapp, Joost van Lingen and Jacco Moorhoff

Numerical Simulation and Validation of Pyrotechnic Smoke Emissions 10

Abdelkarim Habib and Christian Lohrer

Recycling of Global Consumer Fireworks 22

Andrew Tang, Andy Y. F. Tang and Paul Z. J. Peng

Decomposition Kinetics of Pyrotechnic Mixture from Sound-Producing Fire Crackers 33

A. Jeya Rajendran, T. Lekshmana Thanulingam, A. Meisudar and U. Manikandan

Information for Readers 48

Journal of Pyrotechnics

Journal of Pyrotechnics.

8 Aragon Place, Kimbolton, Huntingdon, Cambridgeshire UK

tel: +44 (1480) 878620 email: jpyro@davas.co.uk

Metal–Fluorocarbon Pyrolants. XV: Combustion of two Ytterbium–Halocarbon Formulations

Ernst-Christian Koch,*[a,b] Volker Weiser,[c] Evelin Roth,[c] Sebastian Knapp,*[c] Joost van Lingen[d] and Jacco Moorhoff[d]

[a] NATO Munitions Safety Information Analysis Center (MSIAC), Boulevard Leopold III, B-1110 Bruxelles, Belgium

[b] Technische Universität Kaiserslautern, Erwin-Schrödinger-Str. 52, D-67663 Kaiserslautern, Germany

[c] Fraunhofer Institut für Chemische Technologie, Joseph-von-Fraunhofer-Strasse 7, D-76327 Pfinztal, Germany

[d] TNO Technical Sciences, Lange Kleiweg 137, 2288 GJ Rijswijk, Netherlands

Abstract: *Binary pyrolants based on ytterbium and either polytetrafluoroethylene or hexachloroethane yield a broad stable combustion regime with intense luminous flames. Combustion temperatures have been determined spectroscopically for both pyrolant types. The temperature correlates with the burn rate of the pyrolant. The UV-Vis spectra of the fuel rich pyrolants have been measured and were converted into x,y-color values in the 1931 CIE color diagram. The color obtained with both pyrolant types produce shorter dominant wavelength emission and higher saturation than common BaCl BO_2 emitters.*

Keywords: *Ytterbium, Polytetrafluoroethylene, PTFE, Pyrolant, Burn rate, Combustion Temperature*

Introduction

Some time ago it was reasoned by Sturman that the rare earth metals and their compounds should in principle function as flame color agents.[1] The reason for his assumption was the observation that the individual elements give distinct emissions when introduced as aqueous salt solutions into inductively coupled plasma. Earlier Dumont had found that lanthanum acetylacetonate when used as fuel in an ammonium perchlorate based formulation yields a white flame.[2] Mischmetall and cerium acetylacetonate when used in perchlorate based formulations both yield a faint orange flame.[3] Another important prediction made by Sturman was that either the rare earth metals or their alloys should also yield sparks with colours other than those typically found on the black-body curve. That is, distinct red and green emissions should be accessible at best through use of some of these elements. However apart from the above work the potential of rare earth metals in pyrotechnic formulations has never been investigated.

Recently we have shown that the lanthanide metals samarium (Sm), europium (Eu), thulium (Tm) and ytterbium (Yb) can burn in the vapor phase.[4] This is due to compliance of these metals with Glassman's criterion which requires vaporization temperatures of the metals to be lower than the dissociation temperatures of the corresponding oxides.[4,5] Powdered ytterbium undergoes vapour phase combustion in oxygen and with halogen based oxidizers.[6] A narrow range of ternary mixtures of Yb with polytetrafluoroethylene and Viton® yields extended luminous flames which radiate intensely in the infrared spectral range and outperform standard infrared decoy flare payloads based on Magnesium/PTFE/Viton® (MTV)[7a] in a certain spectral band.[8] In view of the unexpected results of ytterbium based formulations we decided to investigate the combustion behaviour of binary mixtures of ytterbium with polytetrafluoroethylene and hexachloroethane, the latter being the preferred oxidizer in obscurant formulations.[9]

Article Details	***Article No: - 0093***
Manuscript Received:-22/03/2012	***Final Revisions:-10/07/2012***
Publication Date:-11/07/2012	***Archive Reference:-1469***

Experimental details

Warning

Metal–fluorocarbon pyrolants are explosive materials inherently sensitive to electrostatic discharge, heat, flame and impact. These materials when alight yield intense radiation sufficient to cause severe skin burns. In the unconsolidated state the material can undergo deflagration and even shock up to low order detonation in larger quantities (>1 kg).[7b]

All preparations must be conducted in accordance with appropriate national safety regulations. In particular the personnel involved should wear flame-resistant personal protection equipment such as overalls and balaclava made from NOMEX® -III or aluminized PBI® with a facial heat shield. The personnel must be grounded by conductive protective shoes and a wristband, and all equipment and tooling must be grounded as well.[7c]

Ytterbium ingot and powder (99.9% rare earth oxide (REO)), volume median diameter $D[v, 0.5]$ = 3.19 µm, polytetrafluoroethylene, $D[v, 0.5]$ = 7.5 µm and hexachloroethane were all purchased from ALFA AESAR and used without further treatment. The ytterbium ingot was rasped down with a rasp to yield a coarse powder of ~150 µm mean diameter. 5 g batches of the pyrolants were prepared by dry mixing of the components in a 25 ml spherical mixing container made of conductive polypropylene for 30 min at 120 rpm in a tumbling blender. All pellets were pressed at 10 MPa pressure applied for 10 s in a 5.6 mm cylindrical die under safety precautions. Typical sample weight ranged between 1800 and 2000 mg. Pellets were firmly wrapped in transparent adhesive Tesa®-film to protect the lateral surface from flame spreading but to keep the burn front visible. The cylinders were glued with cyanoacrylate glue on small ceramic squares (20 × 20 × 4 mm). The pellets were transferred into a fireproof fumehood with constant venting and ignited with a non-luminous propane torch flame.

For the temperature determination Near infrared-(NIR) spectra were recorded with a PGS-NIR-Spektrometer 2.2 (Carl Zeiss AG, Germany) in the wavelength range λ = 1.0–2.1 µm and calibrated with a technical blackbody heated to 2000 K. Using proprietary ICT-BaM-Code calculated spectra were fitted to the experimental spectra with a least squares fit.[10] The UV-Vis spectra were recorded with a spectrograph Shamrock A-SR-500i-B2 with Andor DU920P-UV-DD-detector (both purchased from Andor Inc. USA). A diffraction grating with 150 lines/mm was used.

The combustion process was recorded with a Panasonic HDC-HS20 with the following settings; aperture: 16; exposure time: 1/8000 s. The accuracy of the burn rate determination is limited by the frame rate of the video camera which is 28 frames/second.

Results and discussion

Pressing densities (ρ_{exp}) greater than 90% Theoretical Maximum Density (TMD) were achieved for Yb/PTFE-compositions containing up to 82 wt% Yb. At higher ytterbium contents the mixtures do not consolidate in the same manner and yield densities of around 87% TMD (Fig. 1). Stable combustion of Yb/PTFE is observed from 62–95 wt% Yb. In this range the combustion rate increases exponentially from about 1 mm s^{-1} to 26 mm s^{-1} at ξ(Yb) ≈ 90 wt% and 87% TMD. With further increasing Yb content the combustion rate decreases again to around ξ(Yb) ≈ 95 wt% as is depicted in Fig. 2. Below 62% Yb ignition of the pyrolant occurs but is followed by rapid

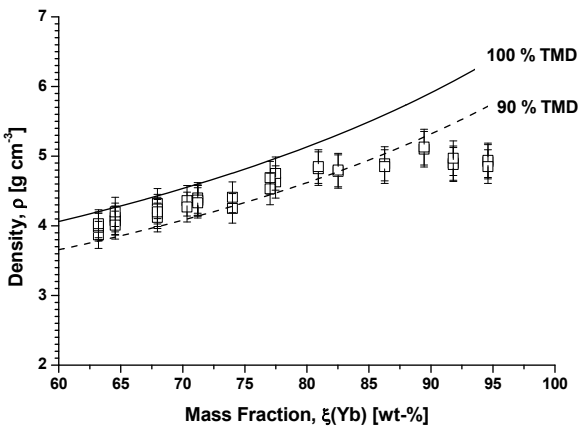

Figure 1. *Experimental density of ytterbium/polytetrafluoroethylene pyrolants and theoretical maximum density (TMD).*

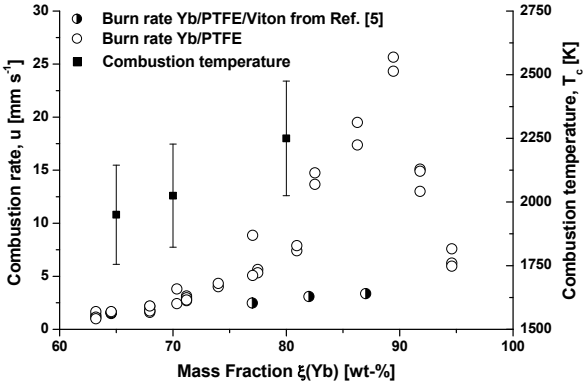

Figure 2. *Combustion rate of Yb-based pyrolants and combustion temperature with bars indicating the scatter of measured data.*

extinction. Above ~95 wt% Yb no cigarette-type burn is observed but the reaction proceeds with very fast glowing of the complete strand followed by delayed scattering of the material, probably due to afterburn with atmospheric oxygen. Thus no proper propagation rate could be determined. The burn rates for binary Yb/PTFE are higher than for three ternary Yb/PTFE/Viton pyrolants reported recently.[8] This is mainly due to higher porosity (eqn 1) of the present samples (φ = 10–20% as opposed to 1–2% for the samples prepared in Ref. 8) which facilitates heat transfer via filtrating combustion.[11]

$$\varphi = 1 - \frac{\rho_{\text{exp}}}{\text{TMD}} \qquad (1)$$

The spectroscopically determined combustion temperature is superimposed for 65, 70 and 80 wt% Yb each on the burn rate in Fig. 2. The measured mean temperatures (1979, 2000 and 2250 K) parallel the combustion rate. A similar behavior has been observed with other metal–fluorocarbon pyrolants recently.[12,13]

Pressing densities (ρ_{exp}) between 80–90% TMD were achieved for Yb/HC-compositions (Fig. 3). Stable combustion of Yb/PTFE is observed from 55–85 wt% Yb. In this range the combustion rate increases exponentially from about 2 mm s^{-1} to 17 mm s^{-1} at ξ(Yb) ≈ 75 wt% and 85% TMD. With further increasing Yb content the combustion rate decreases again to around ξ(Yb) ≈ 85 wt% as is

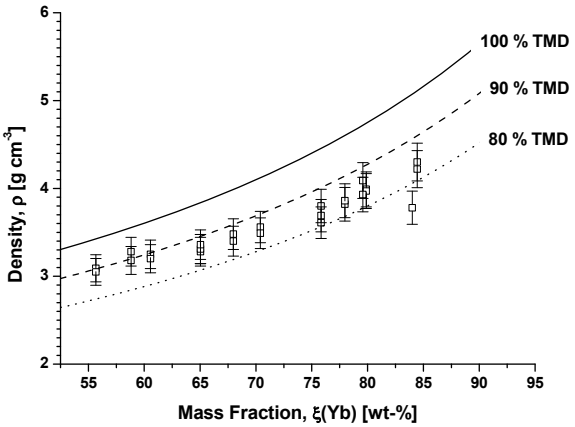

Figure 3. *Experimental density of ytterbium/ hexachloroethane pyrolants and theoretical maximum density (TMD).*

depicted in Fig. 4.

Below 55% Yb ignition of the pyrolant occurred, but was followed by rapid extinction. Above ~85 wt% Yb no cigarette-type burn is observed, but the reaction proceeded with very fast glowing of the complete strand followed by delayed scattering of the material, probably due to afterburn with atmospheric oxygen. The spectroscopically determined combustion temperature is superimposed for 59 and 75 wt% Yb each on the burn rate in Fig. 4. The measured mean temperatures (1700 and 2100 K) nicely parallel the combustion rate.

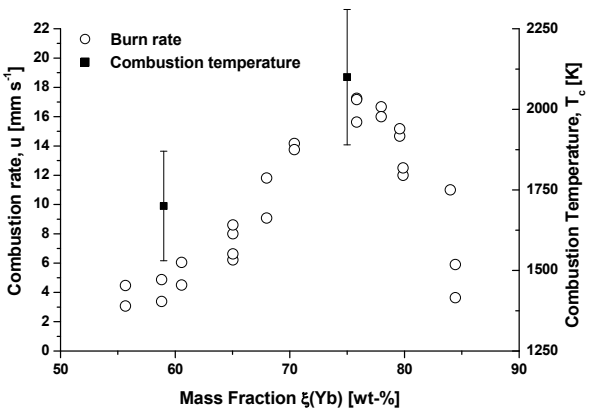

Figure 4. *Combustion rate of Yb-based pyrolants and combustion temperature with bars indicating the scatter of measured data.*

Fuel rich formulations, ξ(Yb) = 70 wt% of both Yb/PTFE and Yb/HC yield a distinct green coloration of the flame that however is partly overlapped by lateral orange soot emissions. Thus the UV-Vis spectra of both pyrolants yield a blackbody continuum superimposed from molecular emissions of Yb species Yb, YbO YbF and YbCl respectively as shown in Fig. 1 of Ref. 6. Subtraction of the blackbody curve yields the principal selective emitters as shown in Fig. 5 and 6.

Normalisation of the spectra, separate convolution

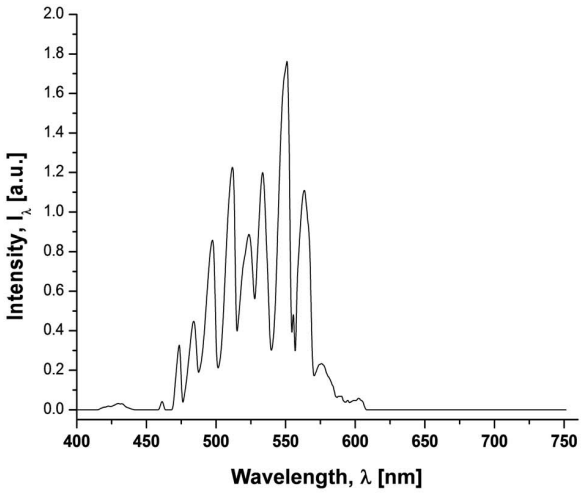

Figure 5. *UV-Vis composite spectrum from YbF, YbO and Yb.*

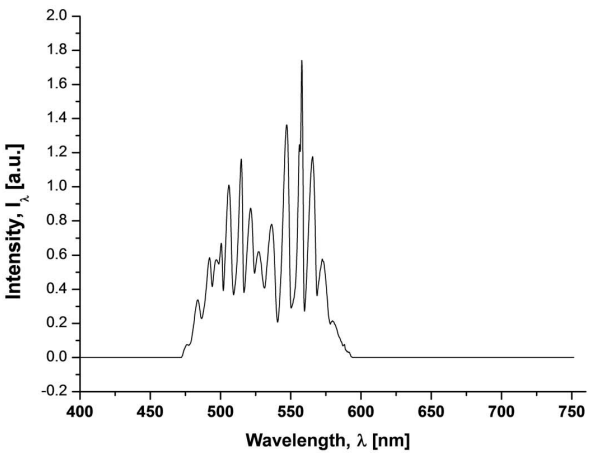

Fig. 6 *UV-Vis composite spectrum from YbCl, YbO and Yb.*

with each of the three tri-stimulus color matching functions,[14] and integration yields the *X*, *Y* and *Z*-values which were converted to *x* and *y*-values as shown in Table 1 and in Fig. 7 and Fig. 8. Dominant wavelength, λ_d, given by ○, and saturation, Σ, were determined graphically.

Due to very similar electronic transitions the

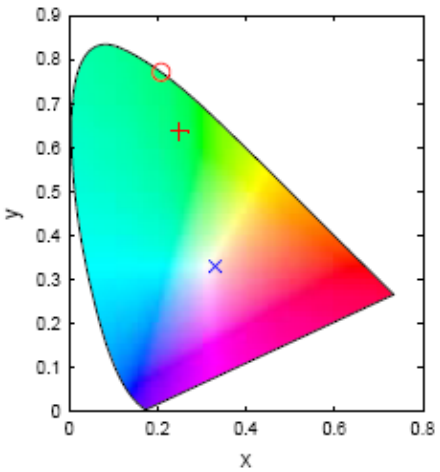

Figure 7. *Color locus of Yb, YbF, YbO composite spectrum,+, dominant wavelength, ○, and white point, ×.*

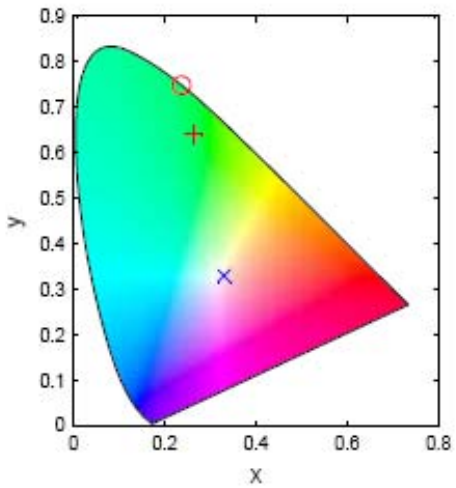

Figure 8. *Color locus of Yb, YbCl, YbO composite spectrum,+, dominant wavelength, ○, and white point, ×.*

Table 1. *Spectral properties of the composite emitter spectra based on Yb and reference data taken from ref. 19*

	Yb/PTFE	Yb/HC	$Ba(NO_3)_2$/Mg/PVC*	B/KNO_3*	B_4C/KNO_3*
λ_d (nm)	537.6	541.2	562.3	559.3	561.9
Σ (%)	69.0	73.8	61.5	55.0	52.0

* plus organic binder for each formulation

emission spectra of YbCl and YbF[15–17] are very similar and hence close color coordinates are obtained. The calculated dominant wavelengths are λ = 537.6 and 541.2 nm, the saturations are 69% and 73% respectively.

For comparison Table 1 shows data for a conventional green star based on barium nitrate ($Ba(NO_3)_2$)/magnesium/PVC/binder, boron(B)/potassium nitrate (KNO_3)/binder and boron carbide (B_4C)/KNO_3/binder[18–20] and the tested Yb/HC and Yb/PTFE. Yb based formulations produce both lower wavelength and more saturated green than common formulations based on barium nitrate boron or boron carbide. This underlines the importance of investigating the rare earth metals as color agents in pyrotechnic flames. Investigation of organic ytterbium salts as fuels in smoke free composition is underway.

Consolidated pellets of freshly rasped coarse ytterbium (150 µm) mixed with PTFE (86/14 wt%) upon ignition with a propane torch yields a loud crackling sound and nice green sparks. A closer view actually shows that the actual sparks are white but are surrounded by areas with green chemiluminescence (Fig. 9).

Conclusion

Ytterbium/polytetrafluoroethylene and ytterbium/hexachloroethane pyrolants yield stable combustion regimes with intense luminous flames ranging from 62–95 wt% and 55–85 wt% Yb respectively. The combustion temperatures derived from NIR spectra for both pyrolant types correlate with the burn rate. The principal emitters in the UV-Vis range have been extracted and converted into x,y-color values in the 1931 CIE colour diagram. The colors obtained with both pyrolant types produce shorter dominant wavelength emission and higher saturation than common BaCl or BO_2 type emitters. Combustion of pyrolant using coarse ytterbium yields intense green sparks.

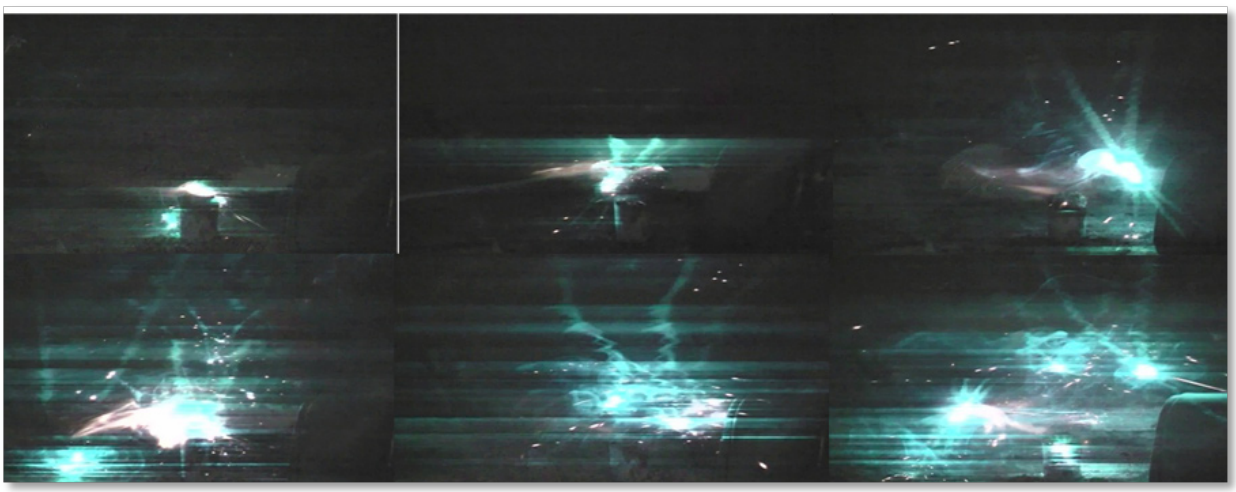

Figure 9. *Crackling combustion of Yb/PTFE (86/14) ejecting green sparks.*

Acknowledgement

Fa. Schwarze Wissenschaftliche Geräte/ Kaiserslautern is thanked for a donation of Yb ingot and powder. Dr. Arno Hahma/Diehl BGT Defence is thanked for determining the particle size distribution of Yb powder.

References

1 B. Sturman, 'The Rare Earths as Possible Flame Color Agents', *Journal of Pyrotechnics*, Vol. 9, 1999, pp. 57–61.

2 J.-L. Dumont, 'Pyrotechnic Compositions for the Production of Coloured Fireworks', EP 0 252 803 B1, 1992, France.'

3 (a) G. C. Shaw and P. S. Shadlesky, 'Smoke/Flame Pyrotechnic Marker Compositions', WASATCH Division, Thiokol Chemical Cooperation, Technical Report AFATL-TR-73-199, September 1973; (b) E.-C. Koch, unpublished work, 2000.

4 E.-C. Koch, V. Weiser, E. Roth and S. Kelzenberg, 'Consideration of some 4f-metals as New Flare Fuels – Europium, Samarium, Thulium, Ytterbium', *42nd International Annual Conference of ICT*, Karlsruhe Germany, June 28 – July 01, 2011, V-1.

5 I. Glassman, 'Combustion of Metals' in *Solid Propellant Rocket Research*, ed. M. Summerfield, Vol. 1 of *Progress in Astronautics and Aeronautics*, 1960, Academic Press, New York, p. 253.

6 E.-C. Koch, V. Weiser, E. Roth, Combustion of Ytterbium Metal, *Propellants Explosives, Pyrotechnics*, Vol. 37, 2012, pp. 9–11.

7 E.-C. Koch, *Metal-Fluorocarbon Based Energetic Materials*, Wiley-VCH, Weinheim, 2012, (a) pp. 166–173; (b) pp. 299-325; (c) pp. 294–296.

8 E.-C. Koch and A. Hahma, 'Metal-Fluorocarbon-Pyrolants. XIV: High Density-High Performance Decoy Flare Compositions Based on Ytterbium/ Polytetrafluoroethylene/Viton®', *Zeitschrift für Anorganische und Allgemeine Chemie*, Vol. 638, 2012, pp. 721–724.

9 E.-C. Koch, 'Metal Halocarbon Pyrolant Combustion' in *Handbook of Combustion*, ed. M. Lackner, F. Winter and W. Agrawal, Vol. 5, Wiley-VCH, Weinheim, 2010, pp. 355–402.

10 V. Weiser and N. Eisenreich, 'Fast Emission Spectroscopy for a Better Understanding of Pyrotechnic Combustion Behavior', *Propellants Explosives, Pyrotechnics*, Vol. 30, 2005, pp. 67–78.

11 Y. V. Frolov and V. G. Korostelev, 'Combustion of Gas-Permeable Porous Systems', *Propellants Explosives, Pyrotechnics*, Vol. 14, 1989, pp. 140–149.

12 E.-C. Koch, A. Hahma, T. M. Klapötke and H. Radies, 'Metal–Fluorocarbon Pyrolants: XI. Radiometric Performance of Pyrolants Based on Magnesium, Perfluorinated Tetrazolates, and Viton A', *Propellants Explosives, Pyrotechnics*, Vol. 35, 2010, pp. 248–253.

13 E.-C. Koch, T. M. Klapötke, H. Radies, K. Lux and A. Hahma, 'Metal-Fluorocarbon Pyrolants. XII: Calcium Salts of 5-Perfluoroalkylated Tetrazoles – Synthesis, Characterization and Performance Evaluation as Oxidizers in Ternary Mixtures with Magnesium and Viton™', *Zeitschrift für Naturforschung B*, Vol. 66b, 2011, pp. 378–386.

14 C. J. Bartleson, 'Colorimetry', in *Color Measurement, Volume 2 Optical Radiation Measurements*, ed. F. Grum and C. J. Bartleson, Academic Press, New York, 1980, pp. 33–148.

15 H. U. Lee and R. N. Zare, 'Chemiluminescent Spectra of YbF and YbCl', *Journal of Molecular Spectroscopy*, Vol. 64, 1977, pp. 233–243.

16 R. F. Barrow and C. H. Chojnicki, 'Analysis of the Optical Spectrum of Gaseous Ytterbium Monofluoride', *Journal of the Chemical Society, Faraday Transactions*, Vol. 75, 1975, pp. 728–735.

17 T. C. Melville, J. A. Coxon and C. Linton, 'High-Resolution Laser Spectroscopy of YbCl: The $A^2\Pi$-$X^2\Sigma^+$ Transition', *Journal of Molecular Spectroscopy*, Vol. 200, 2000, pp. 229–-234.

18 B. V. Ingram, 'Color Purity Measurements of Traditional Pyrotechnic Star Formulas', *Journal of Pyrotechnics*, Vol. 17, 2003, pp. 1–18.

19 J. J. Sabatini, J. C. Poret and R. N. Broad, 'Boron Carbide as a Barium-Free Green Light Emitter and Burn Rate Modifier in Pyrotechnics', *Angewandte Chemie International Edition*, Vol. 50, 2011, pp. 4624–4626.

20 W. Meyerricks and K. L. Kosanke, 'Color Values and Spectra of the Principal Emitters in Colored Flames', *Journal of Pyrotechnics*, Vol. 18, 2003, pp. 52–73.

Numerical Simulation and Validation of Pyrotechnic Smoke Emissions

Abdelkarim Habib and Christian Lohrer
Federal Institute for Materials Research and Testing (BAM) - Unter den Eichen 87, 12205 Berlin, Germany
Email: christian.lohrer@bam.de

Abstract: *This paper aims at evaluating the practicability of an alternative strategy for the classical assessment of possible hazards aligned with the use of theatrical pyrotechnics especially at indoor venues, where the emission of solid reaction products (aerosols) is an important factor for permission for the use of pyrotechnics at stage shows. A CFD model was used to calculate the respective aerosol liberation and dispersion in a specific indoor facility. The results from these numerical simulations were compared with respective aerosol number concentration measurements carried out before, during, and after the burn-off of theatrical pyrotechnic fountains in an examination room, representing a small stage or theatre. The simulation results reveal a fair agreement with the experimental results in general, with the trend to conservatively over-predict the aerosol concentrations at close range to the pyrotechnic article. The time dependent increase and decline of the aerosol concentrations due to the ventilation conditions as observed in the preceding experimental studies could be reproduced in the simulations.*

Keywords: *Theatrical pyrotechnic articles, aerosols, CFD*

Introduction and background

The use of pyrotechnics, such as theatrical articles, for numerous stage and television productions, is globally increasing. New effects and further developments widen this field of application almost every week. Due to this challenging evolution, effective measures are necessary in order to assess the possible risks aligned with the use of such articles, especially during indoor productions, where the audience and the production staff involved are exposed to potentially harmful reaction products of relevant concentrations. Enforcement bodies, e.g. those responsible for the permission for shows including the use of various pyrotechnic articles, are often overwhelmed by the large variety of different special effects and the impacts of the reaction products associated with them. This leads in many cases to a complete rejection of the use of pyrotechnics at a specific venue, just to avoid a situation where the enforcers could be blamed for not acknowledging all possible hazards.

In general, pyrotechnic articles to be placed on the European market fall under the scope of the Directive 2007/23/EC.[1] Theatrical pyrotechnic articles are categorized in the following categories:

- T1: pyrotechnic articles for stage use which present a low hazard, with a further sub-categorization T1 "for outdoor use only", if considered necessary.
- T2: pyrotechnic articles for stage use which are intended for use only by persons with specialist knowledge.

The provisions of that directive assure that these articles are first introduced to a notified body in order to get them appropriately type tested and to demonstrate that all essential safety requirements of this Directive are fulfilled. Furthermore, the articles produced after that EC type-examination must also be in conformity to the initial type. This is usually guaranteed by applying sufficient quality systems for production and/or end product testing (e.g. batch testing), which are subject to regular

Article Details	***Article No: - 0094***
Manuscript Received:- 28/08/2012	***Final Revisions:-20/10/2012***
Publication Date:- 20/10/2012	***Archive Reference:-1506***

inspections by notified bodies, as well.

However, the technical requirements for certification purposes as given in the applicable standard series prEN 16256[2] cover only performance parameters (such as effect dimensions, burning rate and sound pressure level etc.), net explosive content (NEC) and properties of the articles before, during, and after functioning (integrity, stability, unintended explosions, burning matter on ground etc.). Explicit requirements on gaseous or solid reaction products are not included in this standard. The categorization into T1 "for outdoor use only" may only be based on subjective observations of aerosol emissions during the EC type-examination tests by the staff, if all other requirements are met. Furthermore, how does a parallel use of numerous articles, in which all single articles have an indoor use permission, change the authorization of the use of such articles in a theatrical show? A reliable forecast of possible hazards due to the parallel firing of diverse articles is almost impossible for the pyrotechnicians and the enforcement bodies. Confident permission for an envisaged use of theatrical pyrotechnic articles can only be given if all relevant boundary conditions, such as ventilation systems, room geometry or any other protective measures of the affected persons are considered.

Numerical simulations, e.g. computational fluid dynamics (CFD), may play a major key role in future evaluations of such cases, as they can be considered as a possible alternative in this application field to estimate the potential hazard of the use of specific pyrotechnics under defined conditions. CFD is an effective and powerful tool, especially when considering the increasing development of computational processing power in the recent past. In addition, the results from CFD calculations might be integrated in quantified risk assessments (QRA), as well, in order to get a more reliable statement.

The objective of this work was to investigate the practicability of CFD in terms of accuracy of results, time and effort, compared to conventional estimations of the impacts of solid reaction products (aerosols) on a possible indoor use of the respective pyrotechnic articles. This has to be seen in the context of making the authorization process easier for the involved parties: applicants (pyrotechnicians or manufacturers) and enforcement bodies.

For model validation purposes, the respective CFD calculations of this work, using ANSYS CFX V14.0, were compared with the results obtained from previous aerosol measurements during the burn-off of theatrical pyrotechnic articles at an

Figure 1. *Examination room for the measurements carried out by Dutschke et al.*[3]

indoor venue by Dutschke *et al*.[3]

Previous experimental setup – overview

In order to get a reliable validation of the applied numerical model, a case study was chosen in which aerosol emissions during the burn-off of theatrical pyrotechnic articles in a venue-like environment were investigated. These results were previously published by Dutschke *et al*.[3] In this work the authors measured particle number concentrations in the indoor air during and after the burn-off of fountains (amongst others) under defined ventilation conditions. The experiments were performed in a lecture hall with several seating rows, depicting a theatre or stage, see Figure 1.

The room had an overall volume of approximately 718 m^3, offering the following ventilation conditions:

- Outlet – integral: 4400 $m^3\,h^{-1}$ (directly through openings at the room ceiling), and
- Inlet – integral: 4200 $m^3\,h^{-1}$ (directly through circular openings underneath each seat and implicitly through the clearance between both door frames and door panels due to the dominating outlet ventilation conditions).

The theatrical fountains were burned off centered between both laboratory benches, see Figure 1, with the following average properties: burning time 10 s, effect height 3 m, net explosive content (NEC) 32 g.

The local particle number concentrations were measured over minimum 30 minutes at three defined measuring points. The experiments were carried out for each measuring point separately with identical fountains, since only one measuring device (Scanning Mobility Particle Sizer, SMPS) was available. The measuring points in the examination room are shown in Figure 2. The exact same points were also used as validation references

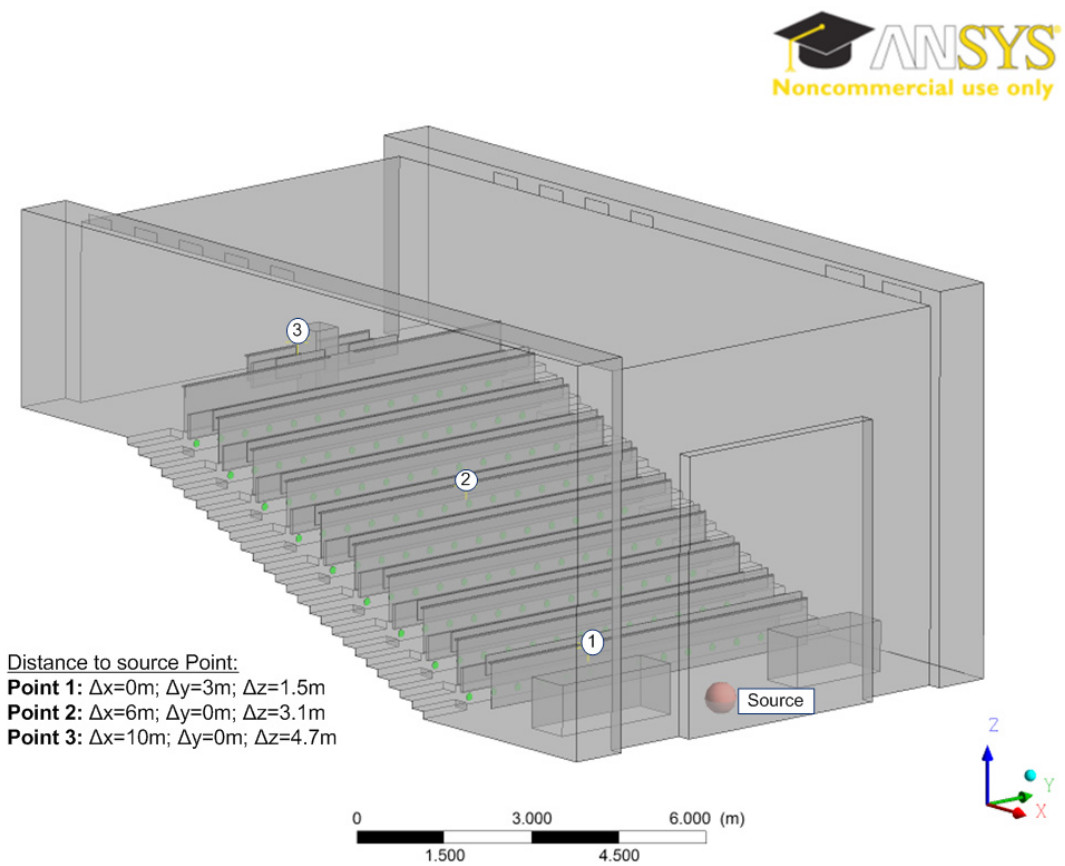

Figure 2. *CAD model of the examination room.*

(monitor points) for the CFD simulations described as follows.

Numerical modeling

The overall goal of the simulations with ANSYS CFX V14.0 was to calculate the liberation of smoke due to the burn-off of a theatrical pyrotechnic fountain and the following transport and dispersion of that smoke in the examination room.

Governing transport equations

The following equations for the conservation of mass, momentum and energy generally apply for three-dimensional, transient, compressible, laminar Newton fluid flows (in Cartesian tensor notation):

Continuity equation (conservation of mass):

$$\frac{\partial \rho}{\partial t} + \frac{\partial \left(\rho u_i \right)}{\partial x_i} = 0$$

Momentum equation: Navier–Stokes (conservation of momentum):

$$\frac{\partial \rho u_i}{\partial t} + \frac{\partial \left(\rho u_i u_j \right)}{\partial x_j} = - \frac{\partial p}{\partial x_i} + \frac{\partial \tau_{ij}}{\partial x_j} + \rho g_i$$

and

$$\tau_{ij} = \eta \left(\frac{\partial u_i}{\partial x_j} + \frac{\partial u_j}{\partial x_i} \right) - \frac{2}{3} \eta \frac{\partial u_i}{\partial x_i} \delta_{ij}$$

Species transport

$$\frac{\partial \rho \mu_k}{\partial t} + \frac{\partial \rho u_i \mu_k}{\partial x_i} = \frac{\partial J_{k,i}}{\partial x_i} + S_{\mu k}$$

and

$$J_{k,i} = -\rho D_k \frac{\partial \mu_k}{\partial x_i}$$

and

$$\mu_k = \frac{m_k}{\sum_{k=1}^{K} m_k}$$

Heat equation (conservation of energy):

$$\frac{\partial \rho h}{\partial t} + \frac{\partial \rho u_i h}{\partial x_i} = \frac{\partial}{\partial x_i} \left(\lambda \frac{\partial T}{\partial x_i} \right) - \frac{\partial}{\partial x_i} \sum_{k=1}^{K} J_k h_k + \frac{\partial p}{\partial t} + u_i \frac{\partial p}{\partial x_i} + \tau_{ij} \frac{\partial u_i}{\partial x_j} + S_h$$

and

$$h = \sum_{k=1}^{K} \mu_k h_k \quad \text{and} \quad h_k = h_{0,k} + \int_{(T)} c_{p_k} \mathrm{d}T$$

Nomenclature

Latin letters	Greek letters
c_p: specific heat capacity	δ_{ij}: Kronecker–Delta
g: gravity	η: dynamic viscosity
h: specific enthalpy	λ: thermal conductivity
i: tensor index (1, 2, 3)	μ_k: mass fraction
j: tensor index (1, 2, 3)	ρ: density
k: species	τ_{ij}: shear stress tensor
m_k: mass	
p: pressure	
S_h: volumic heat flow	
t: time	
T: temperature	
u: velocity	
x: Cartesian coordinate	

Turbulence closure model

Within the numerical simulations of this work, a transient turbulent flow was considered by applying the method of Scale-Adaptive-Simulation (SAS). This approach uses a dynamic function for the turbulent length scale to switch between Reynolds-averaged Navier–Stokes equations (RANS) and the more sophisticated Large-Eddy-Simulation (LES). In contrast to RANS, where all turbulent scales are modeled, LES resolves the large scales ("eddies") and models only small scales. The final resolution of the turbulence is influenced by the mesh size and the time step. SAS basically combines the advantages of both approaches: reasonable CPU times (in case of RANS) and an increased turbulence resolution and accuracy (in case of LES). Further details are given in the ANSYS CFX-Solver Modeling Guide.[5]

Geometry and numerical grid

The examination room which was used in the investigations of Dutschke *et al.*[3] was implemented into the ANSYS-workbench as a ".x_t"-file (parasolid), generated with a common computer-aided design (CAD) tool. The red sphere in Figure 2 indicates the location of the source point simulating the theatrical pyrotechnic fountain. The relevant ventilation openings are located near the ceiling and close to the ground. Eleven outflow ventilation openings are located in the ceiling. Below each bench a row of circular

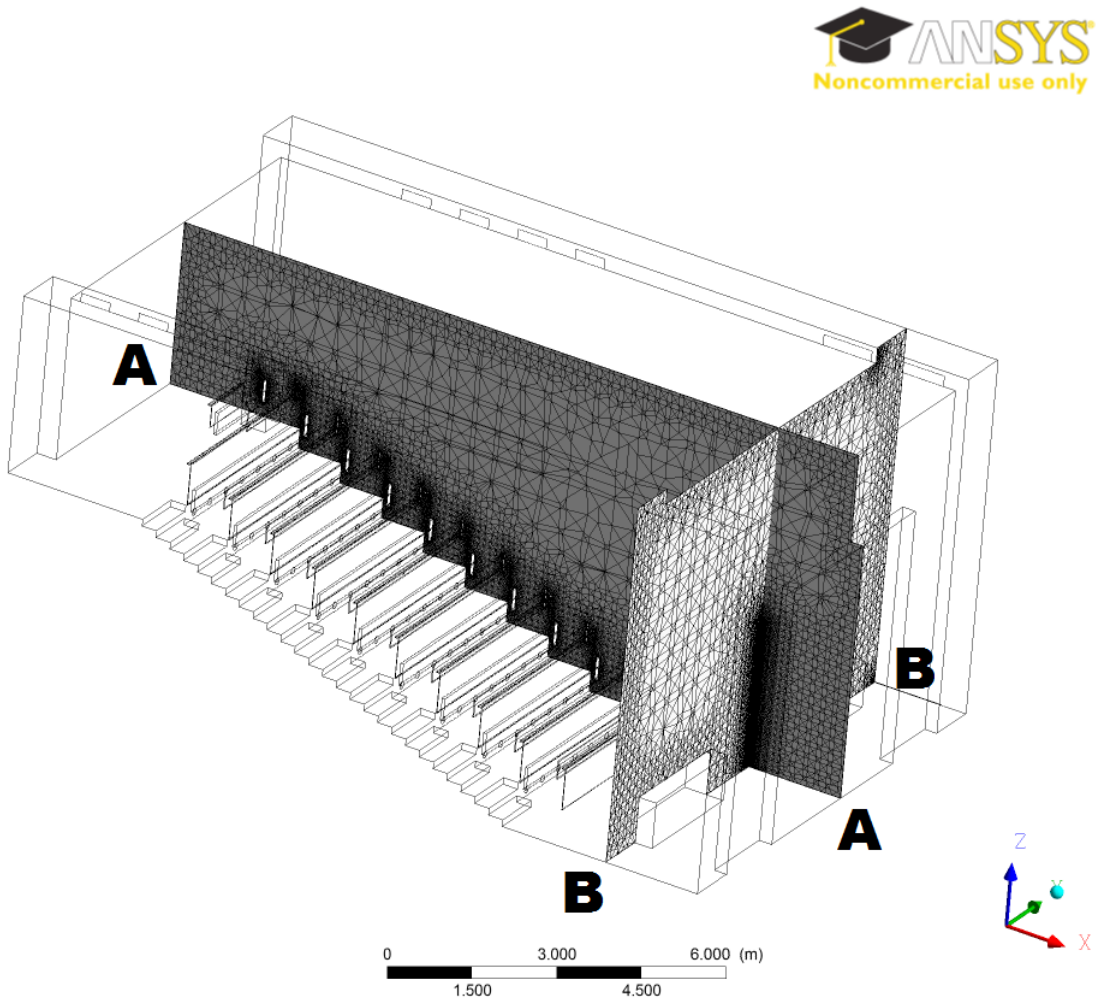

Figure 3. *General view of the domain with two cut planes visualizing the mesh.*

inflow ventilation openings are located. And, thus difficult to visualize in Figure 2 because of its small size, two door clearances with a height of 1 cm and a width of 1 m are respectively placed on the upper floor and the ground floor intersection with the wall on the back right side (in the positive *y*-direction) when looking at Figure 2.

The entire geometry was internally meshed with tetrahedrons (unstructured) and prisms for an appropriate wall boundary layer resolution, resulting in a total number of approximately 3.7×10^6 nodes and 12.77×10^6 elements (consisting of 8.73×10^6 tetrahedrons and 4.04×10^6 prisms).

In Figure 3 a general view of the fluid domain is illustrated with two planes AA and BB showing the mesh. In Figure 4 a detailed view of the AA and BB planes details the refinement in relevant areas. The mesh was refined around the source point (up to the maximum effect height of 3 m), since there were high velocity, temperature and concentration gradients expected, as well as around the inlet and outlet areas. In the same way refinements were made in areas with smaller geometry length scales, as for example around the tables and benches. These refinements related to length scale changes around the tables and benches and the prism layers for the near wall resolution are shown in Figure 5.

Material properties

Air as an ideal gas was defined as the existing ambient material. The density of the air was calculated by the ideal gas law, whereas fixed values of 28.96 kg $kmol^{-1}$ for the molar mass and 1004.4 J $(kg\ K)^{-1}$ for the heat capacity at constant pressure were used. The smoke has been accounted for as an additional variable with a density of 1.3 kg m^{-3}. The advantage of using an additional variable is that no other physical properties have to be defined, although a dispersion of the substance is simulated.

Simplifying model assumptions

To keep the simulations as simple as possible in a first step, physical aerosol effects such as coagulation (particles collide and coalesce with each other, resulting in decreasing particle number concentrations), condensation of vapor phase on particle surfaces (directly affecting the aerosol particle size distribution) and nucleation were neglected. Further details on the numerical simulation of these effects are given amongst others by Hussein *et al*.[4]

The body of the fountain consisting of a cylindrical shape of around 3 cm diameter and 10 cm height was not explicitly resolved by the CAD model. Due to the small size of the fountain body compared to the dimensions of the room, neglecting that object seemed possible without significant effects on the flow in the room aligned with the advantage of simplifying the mesh generation and saving CPU time. Therefore, instead of modeling the body of the fountain, the smoke source was considered as a source point situated at the height corresponding

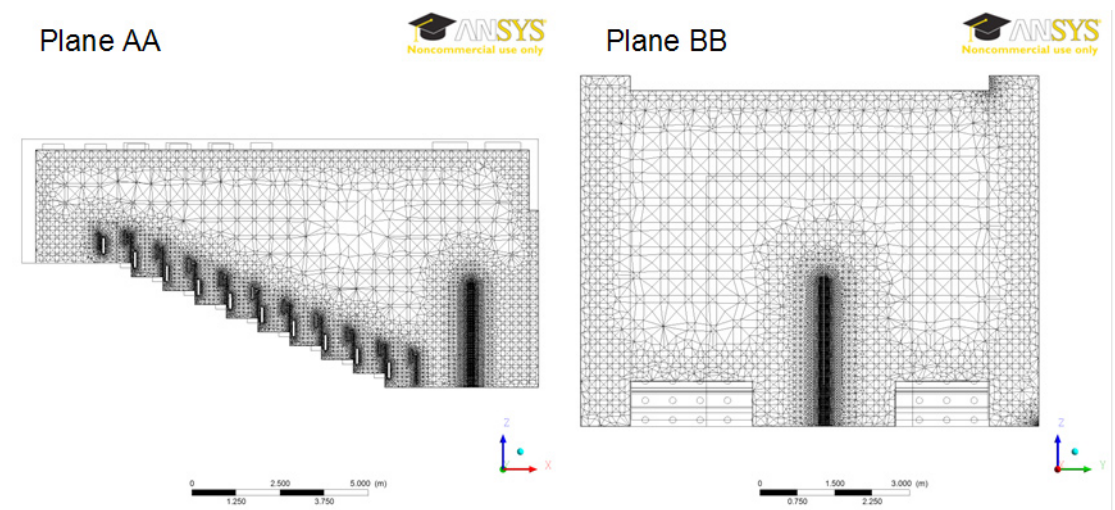

Figure 4. *Cut planes AA and BB for detailed view of the mesh.*

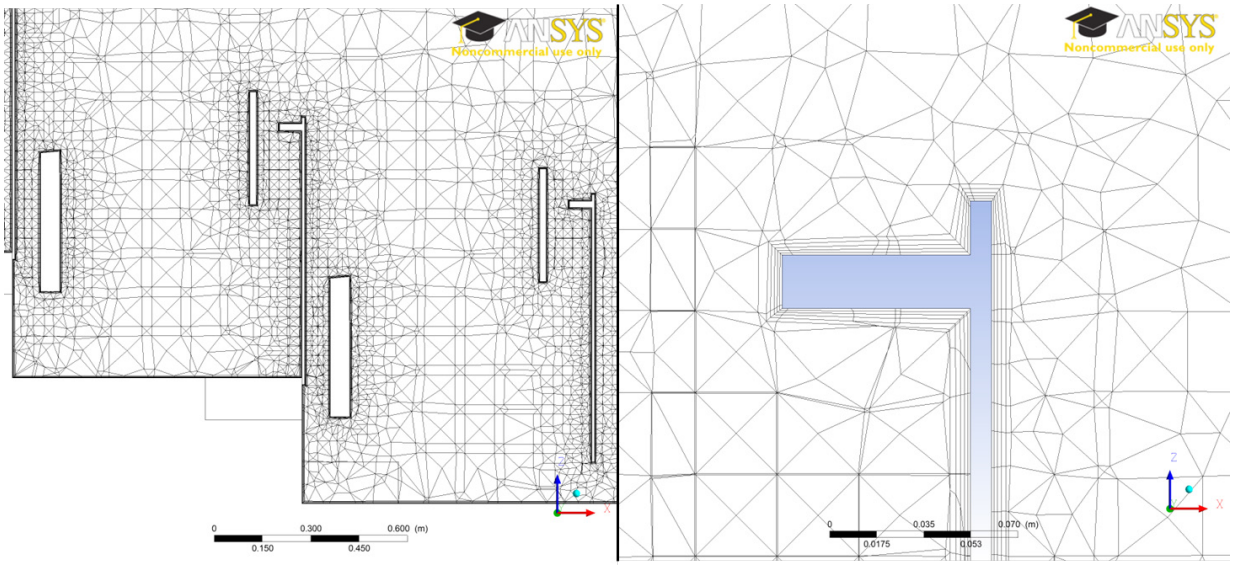

Figure 5. *Detail side view of the mesh around tables and benches with length scale dependent refinement and prism layers.*

to the length of the real fountain.

Furthermore, other minor simplifications of the room geometry were performed for the same reasons of making the mesh generation easier and saving significant CPU time.

Boundary and initial conditions

As the boundary conditions during the experiments did not vary much and were therefore highly reproducible, mean values were used for the simulations. Walls, floor, ceiling, tables and benches were modeled as "wall" boundaries with a "no slip" condition. The source point was defined for releasing a mass fraction of smoke = 1 with a release velocity oriented in the *z*-direction (normal to the ground in direction of the ceiling) of 1.5 m s^{-1}. The latter value corresponds to the measured velocity during the test runs. The mass flow of smoke released was calculated from the known values of released volume and release duration. 8 L of smoke were released during 10 s, corresponding to a volumetric flow of 0.8 L s^{-1}. With an assumed smoke density of 1.3 kg m^{-3}, a mass flow of 0.001 043 kg s^{-1} was determined. The release duration was limited to 10 s according to the real functioning time of the fountain. The air inlet surfaces were modeled as "inlet" boundary conditions, with 0.75 m s^{-1} flow velocity at the circular inlets on the ground and 1.39 m s^{-1} at the door clearances. The air oulet surfaces on the ceiling were set as "outlet" boundary conditions with an outflow velocity of 0.87 m s^{-1}. The velocity values were also calculated from known ventilation and geometric conditions.

As the released smoke is initially at a much higher temperature than the ambient air, the heat transport has been taken into account using the Total Energy model of CFX (see also ANSYS CFX-Solver Modeling Guide[5] for further details).

The simulation was set up as a transient simulation with a total duration of 1860 s. In the first 60 s only the flow in the domain was calculated without any release of smoke, to obtain a flow field in the domain. After that the release was activated for 10 s and during the last 1790 s the dispersion of the smoke was calculated. The time steps used were manually preset as a time step list, with variable time steps varying from 10^{-2} s up to 2.5 10^{-1} s.

Processor properties and software

All CFD simulations were carried out on a high-performance cluster consisting of several nodes. The relevant node contains of 32 cores in total (4 × Magny-Core [8 cores]; AMD Opteron 2.6 GHz/256 GB RAM), of which 24 cores were actually used for the calculations of this work. The program ANSYS 14.0 with its workbench platform was chosen for the CFD simulations of

this work.

The total wall clock time of one case calculation (simulated time of 30 minutes) was around 14 days.

Results and discussion

Although the experimental values were determined in three separate experiments, the simulated values originate from one simulation run. The results shown in the following originate from a simulation with the above described mesh of nearly 13 million cells. Preceding short estimations of the grid influence showed that a highly refined mesh is needed. Unfortunately, further refinements were in principle possible but not on the available hardware. As mentioned before, the concentration of smoke during the experiments was measured at three different locations in the theatre. In Figure 6 the measured time dependent concentrations of smoke are plotted against the simulated values for all three locations.

Although a perfect match of the transient concentrations between the experimental values and the simulations is not reached, it can be seen that the transient dispersion is reproduced quite accurately by the simulations. With only small deviations in time, the simulations predict the rise of the smoke concentration in good agreement with the experimental data. In addition to that, the simulation results detailed in Figure 6 also reveal the decline of the aerosol concentrations due to the comparatively short functioning time of the fountain in combination with the existing ventilation (boundary) conditions. The overall trend is in fair agreement with the experimental results.

Table 1 gives detailed information about the maximum aerosol concentrations and the corresponding time values of the simulations in comparison with the experimental results (see also Figure 6).

The simulations generally tend to over-predict the aerosol concentrations in point 1 and 2 by a factor of roughly 6 and 9, whereas in point 3 an under-prediction by a factor of 5 was observed. However, the simulated times to the respective maximum aerosol concentration peaks correspond very well with the experimental results (Table 1).

In terms of labor protection aspects the time dependent dose information of a certain aerosol exposure of the persons involved is a major key factor when assessing the potential hazards of the burn-off of indoor pyrotechnics. Therefore, the simulated time averaged concentration values over 30 minutes were compared at all three points with the corresponding experimental results published by Dutschke *et al*.[3] As shown in Table 2 the agreement of the time averaged concentration values between simulations and experiments for the points 1 and 2 is better than for the single time dependent maximum values presented in Table 1. However, for point 3 slightly less good agreement on that matter was observed.

The general trend of over-predicting the aerosol concentrations in the close range and under-estimating the concentrations further away from the fountain was not influenced by the time averaging.

The fact that the general prediction type changes from a conservative character at close range to the pyrotechnic article to an optimistic quality further downstream in the examination room may be due to the constant summation of calculation uncertainties, implicitly included in

Table 1 *Transient aerosol concentration characteristics*

Points	Maximum aerosol concentration [mg m^{-3}]		Time to maximum concentration [s]	
	Experiments[a]	Simulations	Experiments[a]	Simulations
1	1.6	9.4	480	436
2 (1st relevant peak)	0.11	1.2	480	481
2 (2nd relevant peak)	0.13	0.8	720	700
3	0.14	0.028	840	870

[a] Values taken from Dutschke *et al.*[3]

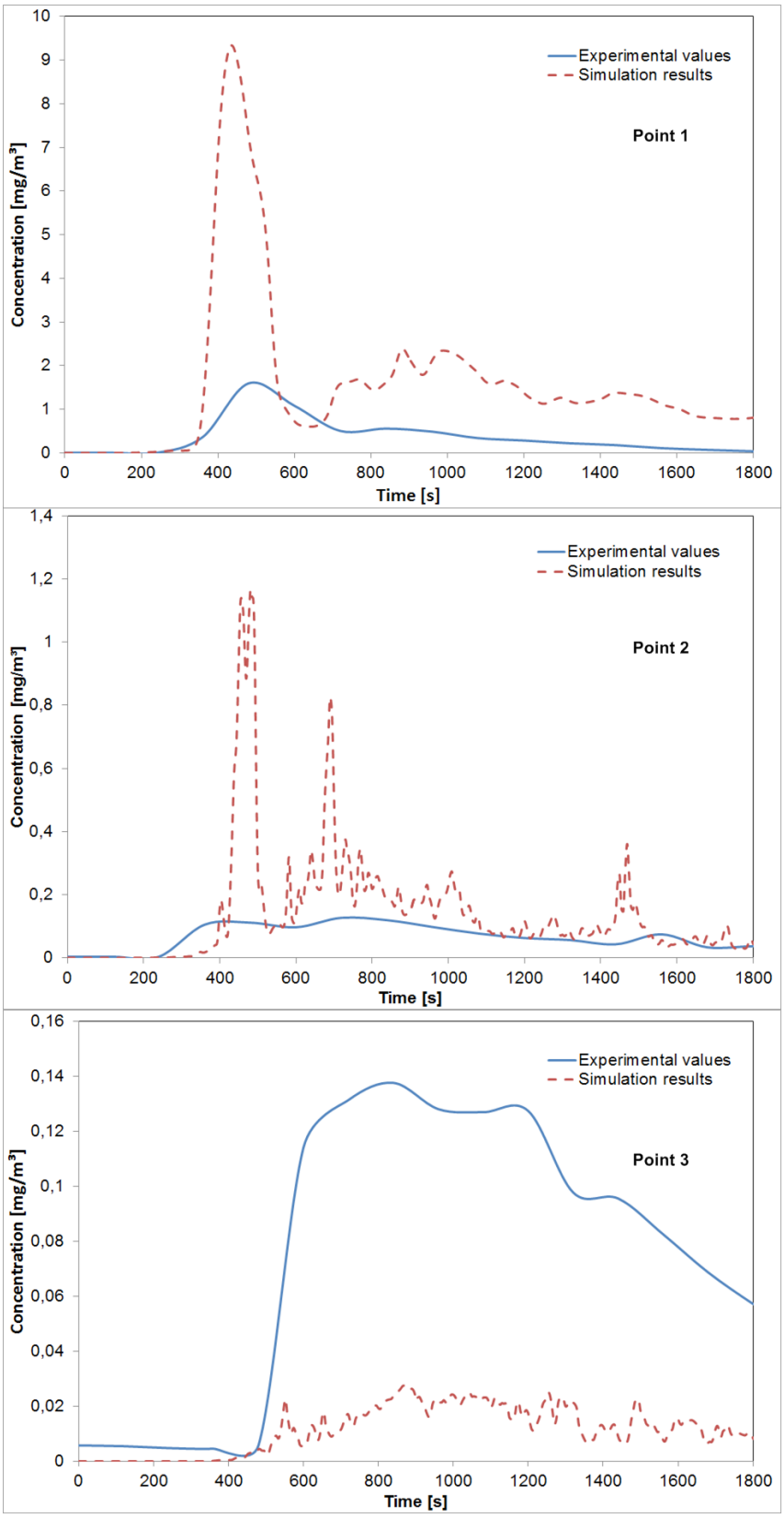

Figure 6. *Measured and simulated aerosol concentrations vs. time at all three measuring/monitor points.*

Table 2. *Time averaged smoke concentrations*

Points	Experimental time averaged concentration (over 30 min) [mg m^{-3}][a]	Simulated time averaged concentration (over 30 min) [mg m^{-3}]
1	0.39	1.62
2	0.07	0.141
3	0.09	0.0115

[a] Values taken from Dutschke *et al*.[3]

the grid refinement, boundary conditions settings and other simplifying model assumptions as mentioned earlier in the text. Using mean values for the boundary conditions instead of the exact values during the experiments could have led to differences in the flow and concentration fields. Furthermore, although the experimental venue was a closed room with regulated ventilation conditions, the simulation omits the fact that one half of the walls of the room consisted of windows. These certainly had an influence on the air and aerosol flow conditions inside the room due to possible effects of sun radiation. In addition to that, the windows might act as heat bridges to the outside, leading to differences in the temperature field influencing the buoyancy and therefore the flow field.

Figure 7 shows the flow vectors during the burn-off of the theatrical fountain 5 seconds after ignition on the centerline cross-section area of the simulated room.

The flow inside the room strongly depends on several aspects like constructional details (e.g. arrangement and dimensions of the chairs and tables) and ventilation conditions etc. Three-

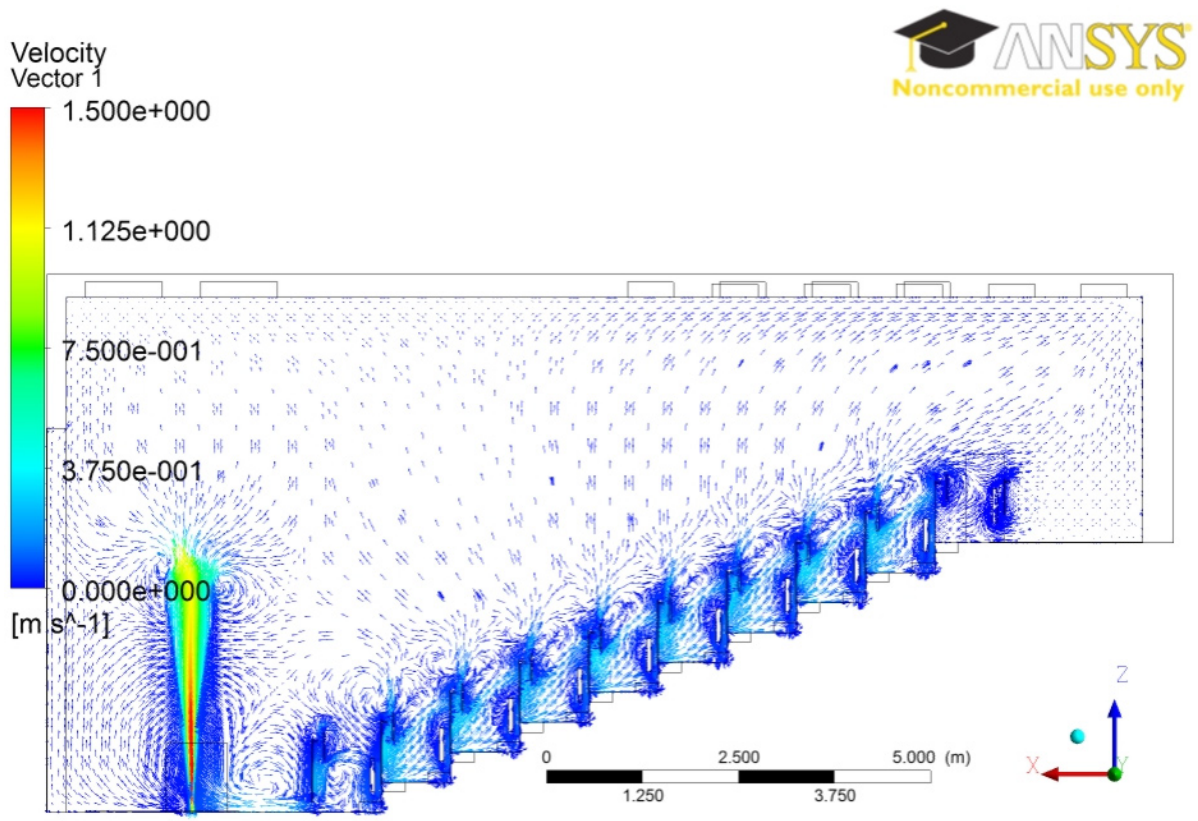

Figure 7. *Flow field in the simulated theatre during the burn-off of a theatrical fountain 5 seconds after ignition.*

dimensional flow measurements inside the room (e.g. with hot-wire anemometry instruments) during the experiments might have given precise flow information in order to improve the estimation of possible calculation uncertainties.

The expansion of the aerosol cloud (for a concentration of 1 mg m^{-3} and higher) due to the dispersion inside the room, as well as the contraction due to the short functioning time of the fountain and the existing ventilation conditions, is displayed in Figure 8.

Summary

This study presents results of the investigations to evaluate the possibility of using common CFD tools for the assessment of possible hazards aligned with the liberation of smoke during the burn-off of pyrotechnic articles in indoor venues. Therefore, a CFD model from ANSYS CFX was taken to simulate the dispersion of aerosols released by the functioning of a typical theatrical pyrotechnic fountain. The calculations were afterwards compared with corresponding preceding experiments.

As a general evaluation it can be stated that the chosen CFD model assumptions led to overall satisfying results compared with the experimental values. The calculations over-predicted the maximum aerosol concentrations in the close range to the pyrotechnic fountain, which corresponds to a conservative hazard estimation. The close range to the aerosol source point plays an important role from the safety point of view, since actors and audience are often in very close proximity to the pyrotechnic effects used in theaters and stage shows. However, a different situation was observed in the far range. With increasing distance from the source point the maximum aerosol concentration values were under-estimated by the simulations in this case, likely due to the summation of calculation uncertainties corresponding to the chosen model assumptions.

In comparison with the accuracy of the maximum concentration values, the transient behavior of the aerosol liberation was much better reproduced by the simulations. The times at which the respective maximum concentration values appeared at all three measuring/monitor points matched the experimental values very well.

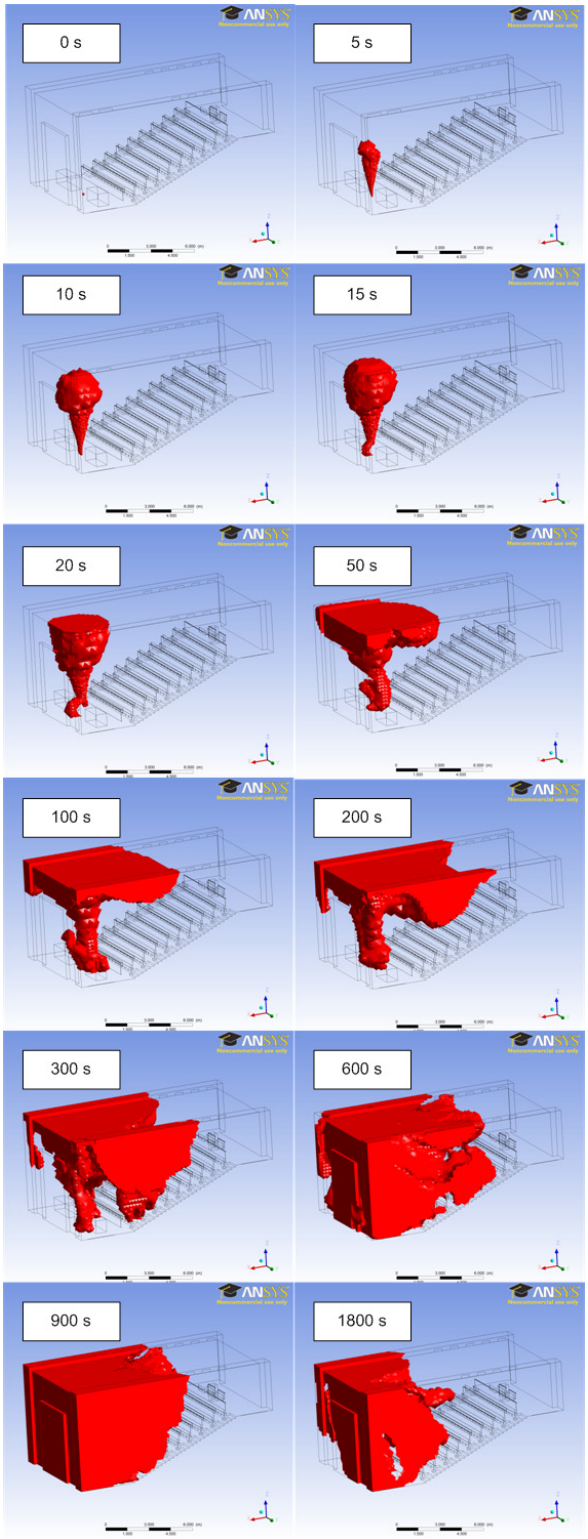

Figure 8. *Time dependent dispersion of the aerosol cloud visualized for a concentration of 1 mg m^{-3} and higher.*

Future simulations might even get better agreements with experimental results, when:

- they are in addition validated with flow measurements,
- more sophisticated numerical methods and approaches are applied,
- physical aerosol effects such as coagulation, condensation of vapor phase on particle surfaces and nucleation are taken into account, and
- a more refined grid is used.

Conclusions

In spite of the high numerical efforts, combined with comparatively long computation times, an application of CFD to estimate potential hazards during the use of pyrotechnics with regards to the liberation of solid reaction products appears to be possible and reasonable. Especially when considering the fast development of computational processing power in the recent years, the application of CFD in this field will become more and more feasible in the future.

CFD results may also play an important role in countries where quantified risk assessments (QRA) are taken into account prior to the permission of the use of pyrotechnics in stage and theatre shows, as they can give information not only on absolute concentration values, but also on transient dispersion effects, basically for every desired venue. These maximum or time averaged concentration values could be compared with national threshold values with regards to labor protection regulations. In particular when using several pyrotechnic articles in parallel during a show, the advantages of CFD may dominate the long computation times.

Another benefit of CFD is the fact that this tool offers the possibility of receiving relevant information, such as concentration, temperature, velocity etc. for every desired location within the 3D fluid domain.

However, several disadvantages of CFD simulations will still exist in the future, regardless of the promising CPU development. These include amongst others the problem or challenge of adequately modeling the flow domain (e.g. construction and import of CAD files), and setting boundary conditions and material properties realistically.

References

1 Directive 2007/23/EC of the European Parliament and of the Council of 23 May 2007 on the placing on the market of pyrotechnic articles, *Official Journal of the European Union*, 14.6.2007.

2 prEN 16256:2012 Standard series for Pyrotechnic articles – Theatrical pyrotechnic articles, consisting of five parts, CEN/TC 212 WG3, 2012.

3 A. Dutschke, C. Lohrer, S. Seeger and L. Kurth, "Towards the reaction products of indoor fireworks", *Proceedings of the 11th International Symposium on Fireworks*, Puerto Vallarta (México), 2009, pp. 66–79.

4 T. Hussein, H. Korhonen, E. Herrmann, K. Hämeri, K. E. J. Lehtinen, and M. Kulmala, "Emission rates due to indoor activities: Indoor aerosol model development, evaluation, and applications", *Aerosol Science and Technology*, Vol. 39, Issue 11, 2005, pp. 1111–1127.

5 ANSYS CFX-Solver Modeling Guide, Release 14.0, November 2011.

Recycling of Global Consumer Fireworks

Andrew Tang, Andy Y. F. Tang and Paul Z. J. Peng
Tian Cheng Pyrotechnics Laboratory, Lihua Village, Yanxi Town, Liuyang City, Hunan, China 410304
Email: atang@tcpyrolab.org

Abstract: *Consumer fireworks is one of the two major fireworks sectors, professional display fireworks and consumer fireworks, in the fireworks industry. It is estimated that consumer fireworks occupy about half of the market share in the global fireworks industry. In terms of packaging materials being used in the consumer fireworks sector, it is definitely true that far more material is being used than in the professional display fireworks sector. This study is a market survey of global consumer fireworks that are on sale in different countries. It was carried out to see what material is being employed in global consumer fireworks and how it is used. The environmental pollution from shooting consumer fireworks is considered from different points of view. Recycling of consumer fireworks has been introduced in China. Innovation in new materials for consumer fireworks is beginning in China.*

Keywords: *Consumer fireworks, recycling, packaging materials, environmental pollution, breakdown of material, NEC, paper*

Introduction

Recycling of fireworks is rarely heard of by consumers or even people working in the fireworks industry. It is commonly accepted that all fireworks are used once and disposed of immediately afterwards, and that it does not matter how and where it is disposed of. In China this is very similar to all types of packaging for consumer goods such as foodstuffs, unless you want to use the packaging again.

The Green Power organization in Hong Kong has conducted an annual survey on people's consumption and celebration habits.[1] The analysis shows the habits of moon cake wastage, and that recycling moon cake packages is still a waste problem. Million of moon cake packages are dumped after the Mid-Autumn Festival. From study data in 2011 September, there were about 47 packaging components used in some types of retail moon cake while the average is 11

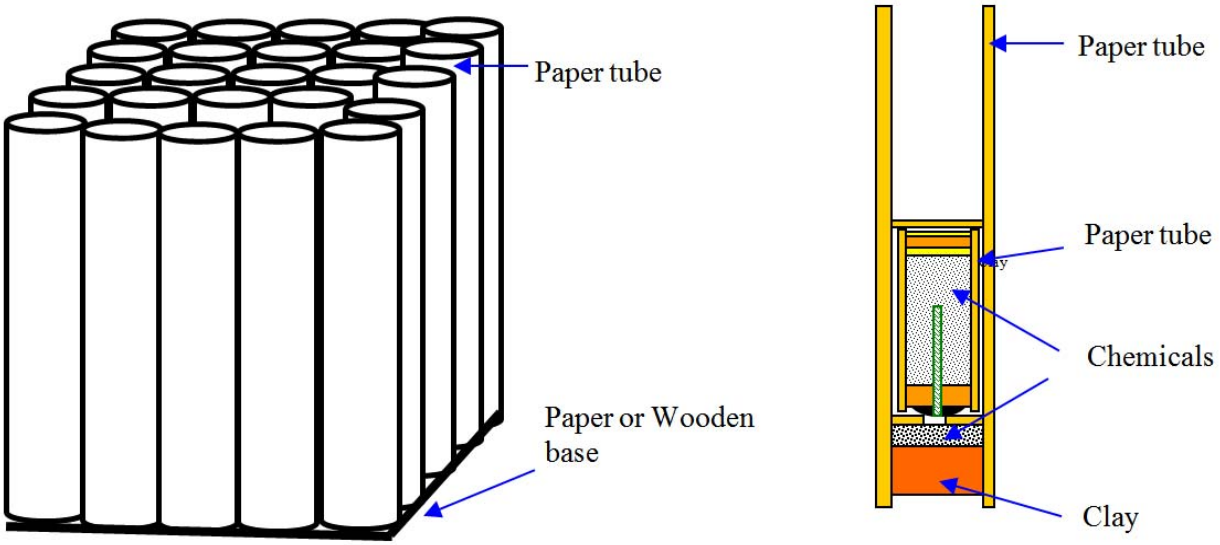

Figure 1. *Structure of consumer fireworks (e.g. cake) showing general inner construction.*

Article Details ***Article No:- 0095***
Manuscript Received:- 29/08/2012 ***Final Revisions:- 13/11/2012***
Publication Date:- 25/11/2012 ***Archive Reference:- 1518***

Table 1. *Distribution of consumer fireworks samples in the study*

Type	No of samples	Range	
		Total mass (g)	NEC (g)
Aerial shells	5	533–606	116–133
Cakes	15	110–10637	16–1124
Firecrackers	9	1.6–857	0.4–107
Fountains	20	16.5–1944	0.4–296
Ground spinner	4	10.6–46.5	2.1–8.4
Helicopters	9	10.3–281.5	3.3–67.4
Magic whip	1	248	134
Missile	3	95–388	18.5–70.4
Novelties	7	2.6–217	1.1–200
Party poppers	5	2.6–354	0.01–0.7
Rockets	5	80.3–359	16.6–150
Roman candles	5	70–740	6.6–107
Sparklers	4	1.3–17.7	0.8–6.9
Others	7	[a]	[a]
TOTAL	99	–	–

[a] Some samples were specially designed and so could not be grouped into different groups. The range of gross weight and NEC were not meaningful.

packaging components.

Normally packaging of consumer fireworks is simple and straightforward. The first ancient Chinese firecrackers contained no packaging, but were simply black powder filled in a piece of bamboo[2] closed at one end. Packaging for the old style fireworks was concerned only with safety and attractiveness. When one looked at a firing site after the consumer had used fireworks, there were torn papers and broken components spread around on the ground. Most of the environmental pollution complaints arising from shooting fireworks concerned air and noise pollution, and much less focused on the left over waste paper and components. This study does not describe the impact caused by pyro-chemicals but focuses on the packing components of consumer fireworks or other material that is left over on the ground after using fireworks. A preliminary similar report was presented .[3]

Consumption of consumer fireworks

All consumer fireworks function using different formulations, combinations and percentages of black powder, stars and effect charges. All of these formulas are composed of chemicals. The functioning of fireworks creates the effects that are its primary performance. As is well known the effects are light, gases and sounds that are produced in the air.[4] During functioning, these chemicals react and generate oxides[5] in the form of small particles, gases, moisture and some burnt debris. These small particles or gases are blown away by the surrounding air. After the functioning of fireworks, all that is left in the air are smoke and gases. There is increasing attention to the environmental impact of these smokes and gases. A lot of studies have been carried out to understand the impact and much research and development is still continuing to eliminate it. Figure 1 shows a typical construction of one type of consumer firework called a battery of shot tubes or the generic term, cakes.

After functioning of fireworks, all that is left over on the ground is packing materials that used to hold chemicals. Since people are allowed to handle and buy consumer fireworks, the main criteria for fireworks packaging are the safety and attractiveness of the fireworks. In the early days of fireworks manufacturing, all packing materials were made mainly of paper and clay. The first firecracker was made of black powder and bamboo. Nowadays plastics and metals have been introduced. Some common items of consumer fireworks are shown in Figures 9 to 12.

Waste from consumer fireworks

Consumer fireworks are always packed or packaged

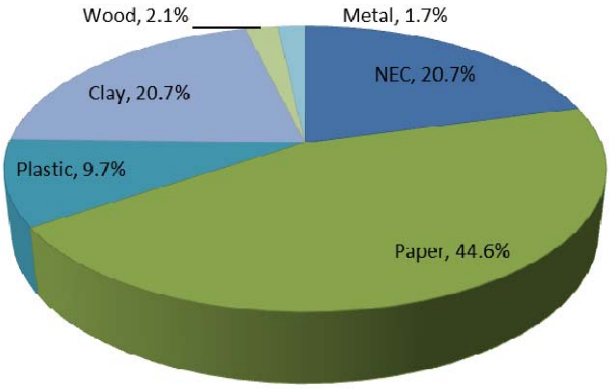

Figure 2. *Percentage of different materials used in consumer fireworks.*

in an attractive manner to draw consumers' attention. Of course manufacturers will ensure the package contains the maximum possible protection to consumers so as to provide safe transportation, handling and functioning.

The sole functioning of fireworks generated by pyrochemicals or net explosive content (NEC) is always the main concern of both consumer and audience. The NEC is composed of chemicals, mainly oxidizers, fuels, and reducing agents. These chemicals are simple and non-toxic or less toxic chemicals such as nitrates, perchlorates, metal powders, sulphur, and some metallic oxides. They are confined inside the paper tube, shell or both to create effects based on different requirements. After ignition of the leading fuse and the subsequent functioning of the firework, all chemicals react to form different forms of oxides. The by-products are water, and energy in forms of light and sound, and smoke. The residue of fireworks that is left on the ground is the waste or containers that used to hold those chemicals.

It is commonly found in China that most used fireworks that are left after firing are collected by waste packers because the material is worth money, similar to other recyclable materials such as glass, metal (aluminum) and plastics. Paper is the most collectible material in recycling of fireworks. It is collected almost immediately after firing in China. Then it is sold to recycling facilities and delivered to paper milling factories where paper is manufactured and supplied back to fireworks factories. See Figures 4 to 7 showing fireworks waste collected in China.

This study focused on the left over waste after the chemicals (NEC) have reacted to form gases and smoke.

Experimental

There were 99 samples randomly selected from different factories manufacturing consumer fireworks for different markets such as the US, EU, China etc. Among these there were different types of consumer fireworks, see Table 1. Their gross weights were measured and they were dismantled. Different materials such as chemicals (NEC), paper, clay, plastic, wood and metal were separated then their weights measured individually. The majority of these consumer fireworks were cakes and fountains because they were commonly available in factories which implies their large market share. Others were rockets, roman candles, small aerial shells, sparklers, helicopters, magic whips and missiles. Their distribution is shown in Table 1.

Results and discussion

Overall average of breakdown of materials in global consumer fireworks

The overall average percentage breakdown of the materials used in global consumer fireworks was 44.6% (w/w) of paper material, 20.7% (w/w) of clay

Table 2. *Breakdown of materials in consumer fireworks by regional market*

Region		NEC (%)	Pa (%)	Pl (%)	Cl (%)	Wo (%)	Me (%)
European		20.8	42.2	5.9	27.5	0.4	2.8
	Max.	63.8	73.5	66.9	70.0	9.6	36.2
	Min.	0.1	22.5	0.1	2.0	9.6	31.6
PRC		16.9	49.4	1.1	32.0	—	—
	Max.	32.0	70.3	7.4	54.0	—	—
	Min.	9.8	30.2	0.1	7.0	—	—
N. America		21.5	44.3	12.7	16.0	3.1	1.6
	Max.	92.0	82.9	64.3	64.7	36.4	57.9
	Min.	0.1	2.7	0.2	2.0	2.8	2.0

Note: No max./min. if there is no average result and absence was not counted as minimum.
NEC = Net Explosive Content; Pa = Paper; Pl = Plastic; Cl = Clay; Wo = Wood; Me = Metal.

Table 3. *Breakdown of materials in different types of consumer fireworks*

Type	NEC (%)	Pa (%)	Pl (%)	Cl (%)	Wo (%)	Me (%)
Aerial shells	21.6	59.4	4.0	14.7	0.0	0.0
Cakes	14.3	39.6	1.7	39.5	4.8	0.0
Firecrackers	14.4	33.1	1.4	50.1	0.0	0.0
Fountains	22.5	49.0	6.7	21.1	0.0	0.0
Ground spinner	27.9	52.4	1.2	17.7	0.0	0.0
Helicopters	23.3	56.0	4.5	14.8	0.0	0.2
Magic whip	54.1	21.8	24.2	0.0	0.0	0.0
Missile	20.1	21.7	56.0	2.1	0.0	0.0
Novelties	31.0	42.6	13.6	4.6	5.2	2.4
Party poppers	0.2	46.6	52.7	0.0	0.0	0.0
Rockets	28.3	44.9	7.1	8.5	10.7	0.0
Roman candles	13.6	72.4	0.0	12.0	1.8	0.0
Sparklers	42.6	19.0	1.3	0.0	0.0	36.9

material, 9.7% (w/w) of plastic material, 2.1% (w/w) of wood material and 1.7% (w/w) of metal material. Chemicals (NEC) occupied 20.7% by weight. See Figure 2.

Breakdown of materials in consumer fireworks by regional areas

If these samples were grouped by different regional areas such as European countries, USA and PRC, the distribution of material was as shown in Table 2. The percentage NEC was highest, 21.5%, for samples for the North American market, while that for the PRC market was the lowest, 16.9%. By contrast, the percentage of paper was highest for the PRC market, 49.4%, and lowest for the European market, 42.3%. In terms of clay material, the PRC market was

Table 4. *Breakdown of materials in different consumer fireworks (excluding NEC from the calculation)*

Type	NEC	Pa-LO (%)	Pl-LO (%)	Cl-LO (%)	Wo-LO (%)	Me-LO (%)
Aerial shells	0	75.8	5.1	18.8	0.0	0.0
Cakes	0	46.2	2.0	46.1	5.6	0.0
Firecrackers	0	38.7	1.6	58.5	0.0	0.0
Fountains	0	63.2	8.6	27.2	0.0	0.0
Ground spinner	0	72.7	1.7	24.5	0.0	0.0
Helicopters	0	73.0	5.9	19.3	0.0	0.3
Magic whip	0	47.5	52.7	0.0	0.0	0.0
Missile	0	27.2	70.1	2.6	0.0	0.0
Novelties	0	61.7	19.7	6.7	7.5	3.5
Party poppers	0	46.7	52.8	0.0	0.0	0.0
Rockets	0	62.6	9.9	11.9	14.9	0.0
Roman candles	0	83.8	0.0	13.9	2.1	0.0
Sparklers	0	33.1	2.3	0.0	0.0	64.3

Table 5. *Breakdown of materials used in cakes*

Materials	Average, grams	Max.	Min.
Gross weight	3376 (100%)	10 637	110
NEC	397.6 (14.3%)	1124	15.6
Paper	1459 (39.6%)	4949	38.4
Plastic	7.3 (1.7%)	48.1	5.1
Clay	1305 (39.5%)	4644	38.4
Wood	207.1 (4.8%)	1400	99.0
Metal	0	0	0

highest, 32.0% and the North American market was lowest, 16.0%. This shows that fireworks sold for the PRC market contain high percentages of paper and clay but least NEC. It was envisaged that the local transportation of fireworks was less expensive than overseas transportation. The packaging of consumer fireworks for the PRC market seems to be more bulky than that for other markets.

Breakdown of materials of different types of consumer fireworks

Different types of consumer fireworks function differently and so they are manufactured using different processes. The materials used, therefore, contain different amounts of different materials. For example sparklers contain a high percentage of metal because of the iron stick although the firecracker does not use metal at all. Hence the percentage breakdown of material is better presented in terms of its type. The breakdown of materials of each type of consumer fireworks is shown in Table 3.

After functioning of these fireworks, all pyro-chemicals reacted giving energetic effects such as sound, light, gases, moisture etc. The leftover materials were paper, plastic etc. Therefore percentages of leftover materials were different and were calculated without the percentage of NEC. The results are shown in Table 4.

Cakes

This type was the largest group of consumer fireworks available in all markets. Due to the similarity of their outer appearance, the sample size was smaller than that for fountains. The number of shot tubes within each sample differed so the performance effect was different too. Hence the higher the number of shot tubes and the higher its effect, the greater the NEC content of the sample. Besides NEC, paper and clay occupied about 80% by weight of this type. The breakdown of materials included mainly paper (39.6%), clay (39.5%) and NEC (14.3%). For a detailed breakdown refer to Figure 3. The maximum and minimum weights of materials are shown in Table 5.

Fountains

The second largest type of consumer fireworks was fountains, which extended from a single tube up to multiple tubes (battery of shot tubes). Due to the varied outer appearance, a larger number of samples was randomly chosen. Besides NEC, paper and clay were still the two main materials used to construct this type of consumer fireworks. More explicitly paper occupied about 50% by weight of its gross weight. The average waste from fountains consisted of paper 49.0%, clay 21.1% and plastic material 6.7% by weight. For a detailed breakdown refer to Figure 3. The maximum and minimum weights of material are shown in Table 6.

Table 6. *Breakdown of materials used in fountains*

Materials	Average, grams	Max.	Min.
Gross weight	375.8 (100%)	1,944	40.0
NEC	70.9 (22.5%)	296.3	0.4
Paper	171.9 (49.0%)	788.7	12.4
Plastic	13.1 (6.7%)	110.7	0.7
Clay	115.9 (21.1%)	865.4	2.1
Wood	3.3 (0.3%)	65.2	0
Metal	0.0 (0.0%)	1.8	0

Table 7. *Breakdown of materials in helicopters*

Materials, grams	Average	Max.	Min.
Gross weight	116.7 (100%)	282	10.3
NEC	24.8 (23.3%)	67.4	3.3
Paper	64.3 (56.0%)	175.5	6.2
Plastic	4.8 (4.5%)	15.6	0.02
Clay	21.3 (14.8%)	79.2	0.7
Wood	0 (0%)	0	0
Metal	0.6 (0.2%)	6.1	0

Table 8. *Breakdown of materials in novelties*

Materials, grams	Average	Max.	Min.
Gross Weight	114.4 (100%)	217	2.6
NEC	37.5 (31.0%)	200	1.1
Paper	58.5 (42.6%)	160	0.5
Plastic	9.5 (13.6%)	37.9	0
Clay	5.7 (4.6%)	19.5	0
Wood	0.1 (5.2%)	0.9	0
Metal	2.3 (2.4%)	8.6	0

Table 9. *Breakdown of materials in firecrackers*

Materials, grams	Average	Max.	Min.
Gross weight	109.8 (100%)	857	1.6
NEC	13.2 (14.4%)	106.6	0.4
Paper	63.5 (33.1%)	530.4	0.4
Plastic	2.2 (1.4%)	18.7	0
Clay	29.8 (50.1%)	191	0.8
Wood	0 (0%)	0	0
Metal	0 (0%)	0	0

Helicopters

This type of consumer fireworks contained different designs. Metal and plastic materials were also introduced. There were 9 different samples randomly selected from factories. Besides NEC, the first two materials were paper, 56%, and 14.8% of clay. The lowest was plastic, 4.5% by weight. For a detailed breakdown refer to Figure 3. The maximum and minimum weights of material are shown in Table 7.

Novelties

This type contained all 5 different materials because the type was more attractive to younger consumers on account of their appearance rather than their pyrotechnic effects. There were 7 different samples randomly selected from factories. Besides NEC, the first two main materials were paper, occupying 42.6% by weight and plastic, 13.6% by weight. For a detailed breakdown refer to Figure 3. The maximum and minimum weights of material are shown in Table 8.

Firecrackers

This type of consumer fireworks was the traditional

Table 10. *Breakdown material of rockets*

Materials, grams	Average	Max.	Min.
Gross weight	192.0 (100%)	359	80
NEC	56.0 (28.3%)	150	16.6
Paper	84.5 (44.9%)	195.3	34.0
Plastic	15.1 (7.1%)	58.2	0.6
Clay	21.1 (8.5%)	84.4	4.1
Wood	14.4 (10.7%)	34.4	0
Metal	0 (0%)	0	0

Table 11. *Breakdown material of small aerial shells*

Materials, grams	Average	Max.	Min.
Gross weight	573.1 (100%)	606.5	533.0
NEC	123.6 (21.6%)	133.4	116.2
Paper	340.4 (59.4%)	382.4	313.5
Plastic	22.9 (4.0%)	28.4	20.5
Clay	84.3 (14.7%)	98.1	64.3
Wood	0 (0%)	0	0
Metal	0.2 (0.1%)	0.3	0

type. Due to the manufacturing process they did not vary too much, and the materials used were mostly the same as before. There were 9 different samples randomly selected from factories. This type of consumer fireworks was separated into batteries of firecrackers (or firecrackers on strings) and individual firecrackers. Therefore there was a large spread in the results. Besides NEC, the first two main materials were paper, occupying 33.1% by weight and clay, 50.1% by weight. This group of consumer fireworks did not contain wood nor metal materials. However it contained the highest percentage of clay among all types of fireworks. It was envisaged that firecrackers provided simply a noise effect, a bang, which was mainly generated by using clay confinement. For a detailed breakdown refer to Figure 3. The maximum and minimum weights of material are shown in Table 9.

Rockets

There were 5 different samples randomly selected from factories. Besides NEC, the first two main materials were paper, occupying 44.9% by weight and wood, 10.7% by weight. This type contained the highest percentage of wood among all types, because all the rocket sticks were of wood. For a detailed breakdown refer to Figure 3. The maximum and minimum weights of material are shown in Table 10.

Small aerial shells

This type of consumer fireworks was small reloadable aerial shells of less than 1.75 inches diameter. They could be repeatedly loaded into a launch tube and fired one after another. The item is commonly available in the American market. Besides NEC, the first two main materials were paper, occupying 59.4% by weight and clay, 14.7% by weight. For a detailed breakdown refer to Figure 3. The maximum and minimum weights of material are shown in Table 11.

Roman candles

There were 5 different sample randomly selected from factories for this type of consumer fireworks. Besides NEC, the main two materials were paper, occupying 72.4%, and clay, 12.0% by weight. For a detailed breakdown refer to Figure 3. The maximum and minimum weights of material are also shown in Table 12.

Party poppers

This type of consumer fireworks contained 5 different samples but were all very similar to each other. Besides NEC, the main two materials were plastic, occupying 52.7% by weight and paper, 46.6% by weight. For a detailed breakdown refer to Figure 3.

Table 12. *Breakdown of materials in roman candles*

Materials	Average, grams	Max.	Min.
Gross weight	310.2 (100%)	740	70
NEC	44.3 (13.6%)	107	6.6
Paper	226.2 (72.4%)	544	50.0
Plastic	0 (0%)	0	0
Clay	37.1 (12.0%)	88.5	2.9
Wood	2.0 (1.8%)	1.8	0
Metal	0 (0%)	0	0

Table 13. *Breakdown of materials in party poppers*

Materials	Average, grams	Max.	Min.
Gross weight	127.3 (100%)	354	2.6
NEC	0.3 (0.2%)	0.7	0.01
Paper	61.1 (46.6%)	173	1.0
Plastic	65.7 (52.7%)	180	1.6
Clay	0 (0%)	0	0
Wood	0 (0%)	1.8	0
Metal	0 (0%)	0	0

Table 14. *Breakdown of materials in sparklers*

Materials	Average, grams	Max.	Min.
Gross weight	12.7 (100%)	17.7	1.3
NEC	4.6 (42.6%)	6.6	0.8
Paper	3.1 (19.0%)	6.9	0
Plastic	0.2 (1.3%)	0.8	0.1
Clay	0 (0%)	0	0
Wood	0 (0%)	0	0
Metal	4.7 (36.9%)	9.5	0.5

Table 15. *Breakdown of materials in missiles*

Materials	Average, grams	Max.	Min.
Gross weight	242.7 (100%)	387.6	95.0
NEC	48.2 (20.1%)	70.4	18.5
Paper	48.9 (21.7%)	64.2	23.0
Plastic	139.0 (56.0%)	243.0	53.3
Clay	6.2 (2.1%)	9.6	0
Wood	0 (0%)	0	0
Metal	0 (0%)	0	0

The maximum and minimum weights of material are also shown in Table 13.

Sparklers

This type of consumer fireworks contained 4 different samples. It was the type of consumer fireworks containing the largest amount of metal material. Besides NEC, the main two materials were metal, occupying 36.9% by weight, and paper, 19.0% by weight. For a detailed breakdown refer to Figure 3. The maximum and minimum weights of material are shown in Table 14.

Missiles

This type of consumer fireworks contains 3 different samples only. Besides NEC, the main two materials were plastic, occupying 56.0% by weight and paper, 21.7% by weight. For a detailed breakdown refer to Figure 3. The maximum and minimum weights of material are shown in Table 15.

Magic whip

This is the only group containing 1 sample only, because such samples are not common. Besides NEC, the main two materials were plastic, occupying 24.2% by weight and paper, 21.8% by weight. A detailed breakdown is shown in Figure 3.

Conclusion

Most of the waste from consumer fireworks consisted of paper and clay materials after functioning which were 44.6% and 20.7% respectively by weight. If only leftover materials were counted (deducting NEC, 20.7%) these two materials occupied 56.2% and 26.1%, a total of 82.3%. Wood occupies 6% and metal occupies 3%. All of them are recyclable easily. Therefore most consumer firework packaging (waste from fireworks) is collected by pickers who sell to recycling facilities, see Figures 4 to 7, for recycling of paper. Plastic is the most arguable material as it depends on which type of plastic it is. The percentage of plastic material is about 9.7% by weight (or 9% by weight of leftovers) among all consumer fireworks. Among these recycling materials, the one with the greatest impact on environmental pollution is plastic material. Most of the plastic found in the study was PVC and PE.

If packaging used more environmentally friendly materials, the percentage of recycling would increase, and it would have less impact on the environment. Some factories have started to develop the use of new reusable materials in the manufacturing of fireworks, such as plastic tubes for reloadable aerial shells or some new materials which are biodegradable in the environment, as shown in Figure 8. As a general trend, manufacturers have become aware of the challenge as well as the opportunity offered by the environmental impact caused by fireworks.

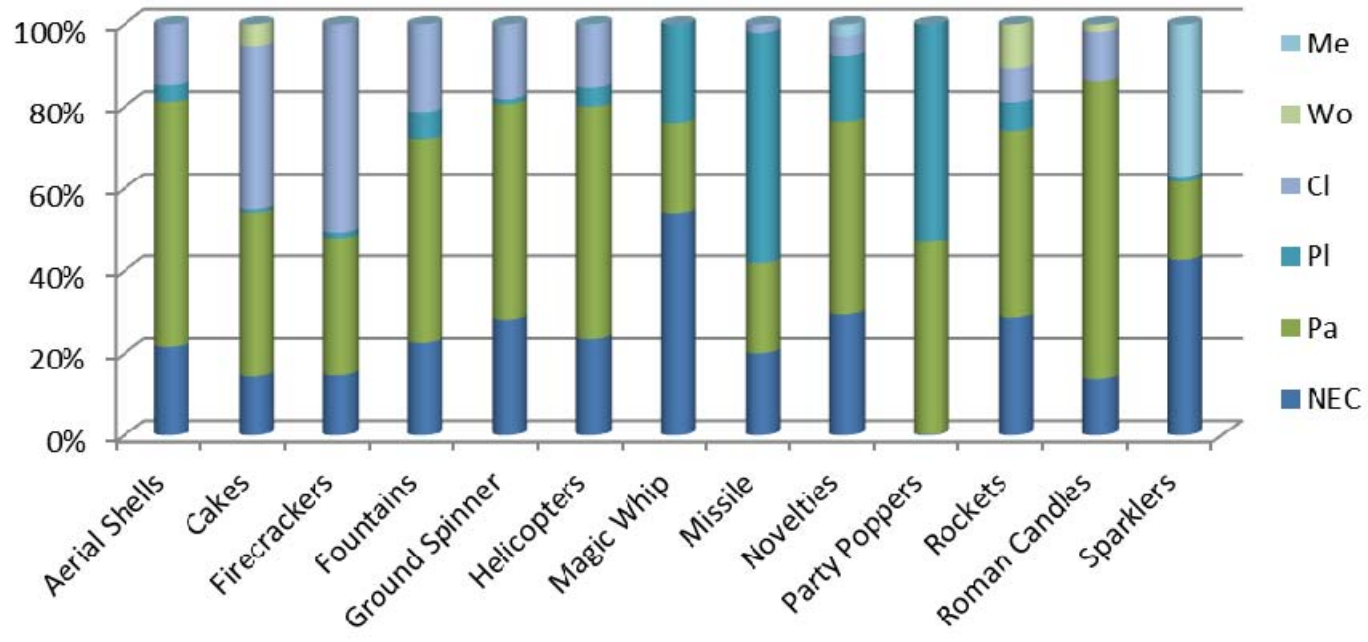

Figure 3. *Material used in different types of consumer fireworks by percentage.*

Figure 4. *Waste fireworks collected in recycling shops in Liuyang City, Hunan, China.*

Figure 5. *Trash paper from different packaging consumer products.*

Figure 6. *Recycling paper by mixing trash paper and fibers before milling.*

Figure 7. *Finished recycled paper.*

Figure 8. *Innovative material to replace paper and clay in manufacturing cakes*

Figure 9. *Some examples of consumer fireworks: (a) missile; (b) helicopter; (c) firecrackers; (d) novelty.*

Table 16. *Breakdown of materials in magic whip*

Materials	Average, grams	Max.	Min.
Gross weight	247.5 (100%)	0	0
NEC	133.8 (54.1%)	0	0
Paper	53.9 (21.8%)	0	0
Plastic	59.8 (24.2%)	0	0
Clay	0(0%)	0	0
Wood	0 (0%)	0	0
Metal	0 (0%)	0	0

References

1. Green Power, Hong Kong, *Survey on Consumption and Celebration Habits during Mid-Autumn Festival*, September 13, 2011.

2. N. J. Lo, *Manufacturing and Safe Management of Fireworks*, Hunan Scientific Technology Publisher, 1987.

3. Andrew Tang, *Recycling of Consumer Fireworks*, 13th ISF Malta 2012.

4. Ronald Lancaster, *Fireworks – Principles and Practice*, 4th edition (2006).

5. Michael S. Russell, *The Chemistry of Fireworks*, RSC Publishing, 2000.

Decomposition Kinetics of Pyrotechnic Mixture from Sound-Producing Fire Crackers

A. Jeya Rajendran,[a*] T. Lekshmana Thanulingam,[b] A. Meisudar[2] and U. Manikandan[b]

[a] Department of Chemistry, Loyola College, Nungambakkam, Chennai-600034, India.
Email: jeyarajendran@yahoo.com

[b] Fireworks Research and Development Centre, Petroleum and Explosives Safety Organisation, Anayoor village, Sivakasi -626124, India. Email: tlthanulingam@yahoo.co.in

Abstract: *Dynamic, non-isothermal analysis of the pyrotechnic mixture of a sound-producing fire cracker, $KNO_3/Al/S/H_3BO_3$, was carried out under N_2 atmosphere by using a simultaneous thermogravimetric and differential thermal analyser. Intermediates and the residue formed in each stage of thermal decomposition of the pyrotechnic mixture were characterised by X-ray diffraction analysis and the most probable reaction pathway was proposed. Thermogravimetric (TG) and differential thermogravimetric data (DTA) were used for the interpretation of the mechanisms and kinetics of decomposition by means of a model-fitting method, the Coats–Redfern equation, and model-free methods, the Arrhenius and Kissinger methods. The values of activation energy (E) were calculated as 11–16 kJ mol^{-1}, 24–53 kJ mol^{-1} and 15–56 kJ mol^{-1} for stages I, II and III respectively by the model-fitting method, with the Avrami–Erofe'ev model (A2), two-dimensional model, nucleation and growth mechanism. The pre-exponential factor (ln A) of each stage of thermal decomposition at various linear heating rates was calculated and the probable decomposition mechanism was proposed for the first decomposition step as the expulsion of sulphur, and the second and third decomposition steps as the conversion of aluminium to alumina are obtained. Similarly, the reaction was also found to be first order.*

Keywords: *pyrotechnics, fireworks, thermal analysis, activation energy, Coats–Redfern equation.*

Introduction

Pyrotechnic compositions are mixtures of reducing and oxidising chemicals that are capable of undergoing self-sustained combustion. The reducing agent is often referred to as fuel. In general, the composition of fireworks is a mixture of sulphur or phosphorus, perchlorate or nitrate and pure aluminium powder.[1] The pyrotechnic mixtures are sensitive to impact, friction, electrostatic thermal energy and auto-ignition temperature. The composition of fireworks should possess high sensitiveness to flame and low sensitiveness to other factors like impact, friction and electrostatic energy.

A pyrochemical reaction characteristically produces heat energy which may be useful directly as thermal energy or more usually as light, sound and kinetic energy to achieve a desired effect. This reaction must not begin to proceed as soon as the pyrotechnic composition is mixed and the spontaneity is prevented by the characteristic property of pyrotechnic compositions, the 'activation energy' barrier. An externally applied flame can initiate the ignition process by supplying the activation energy to the composition. If the activation energy barrier is low, accidental ignition will be more likely because a small amount of mechanical or electrostatic energy can cause ignition of the composition. Different oxidizers are used in the pyrotechnic mixture in order to get the desired effect of the fireworks and the parameter, energy of activation, can be used to check which oxidizer in the pyrotechnic mixture can be

Article Details ***Article No:- 0096***

Manuscript Received:- 03/12/2012 ***Final Revisions:- 20/12/2012***

Publication Date:- 07/01/2013 ***Archive Reference:- 1526***

effective for a particular type of fireworks.

Potassium permanganate and phosphorus have low activation energy and therefore could not be used in the composition of pyrotechnics in the firework industry. Activation energy is not only affected by the nature of the oxidizers and the igniter but the same materials in different combinations may also lead to low activation energy creating a significant hazard. Accidental ignition during processing or spontaneous ignition during storage is the major problem in the fireworks industry which is the main focus of our work. The mechanism involved in the combustion and explosion reaction of pyrotechnic mixture in a firework is entirely different compared to the spontaneous ignition reaction of pyrotechnic mixture during storage.

In the firework industry, after mixing the ingredients, the pyrotechnic mixture is used to fill contrivances. Cardboard boxes are used for cake bombs and atom bombs; tubes are used for Chinese crackers and cones are used for flower pots and the combustion reaction is carried out in a confined way in the fire crackers. Differential Scanning Calorimetry (DSC) and Accelerating Rate Calorimetry (ARC) are suitable techniques for calculating thermodynamic parameters in a closed system as well as to interpret the mechanism. Simultaneous thermal analysis (TA), thermogravimetric (TG) and differential thermal analysis (DTA) can be used for studying the decomposition kinetics of the pyrotechnic mixture for ignition or explosion during storage.

The parameters that influence the thermal behaviour are particle size distribution, purity and moisture content of the chemicals etc. Decrease in particle size of KNO_3 had an adverse effect on sensitivity to both impact and friction to a greater extent than the particle size of Al,[2] and set the lowest onset temperature for the exothermic activity. The heat content from the exothermic activity was also found to vary with particle size.[3] Decreasing the particle size from micro-size to nano-size pyrotechnic mixture was found to produce sound effectively and it was reported that a smaller amount of pyrotechnic mixture is required to produce the allowed sound level of 120–125 dB(A) as prescribed by the Govt. of India[4] on using a nano pyrotechnic mixture.[5] Although it is expected that the particle sizes create large interfacial areas and increased number of atoms at the particle interface which on ignition lead to a higher heat of reaction, the various physical and chemical processes occurring concomitantly and competitively may affect the process.

The effect of particle size of the pyrotechnic mixture on the heat of reaction was carried out using DSC[5] and ARC.[3] Many studies have been carried out on the factors affecting the sound level produced from the fire crackers[5] and especially on particle size[6–8] which played a key role in producing the sound level from the fire crackers. Kinetic parameters for all the stages of decomposition have not been reported so far. In the present work, thermal analysis was carried out to deduce the decomposition pattern of the pyrotechnic mixture under well controlled conditions by TGA and DTA techniques. Kinetic parameters for different decomposition stages are derived from the results and the conclusions drawn from them are presented. Importance is given to calculating the kinetic parameters, energy of activation (E) and pre-exponential factor ($\ln A$) by following model-fitting methods, the Coats–Redfern equation, and model-free methods, the Arrhenius and Kissinger methods. Data for energy of activation related to different proportions of pyrotechnic composition and for commonly used mixtures of oxidizers and igniter have not been reported in the literature. An attempt is made to calculate the energy of activation for pyrotechnic mixtures with different oxidizers in varying compositions.

The present work focuses on the most commonly used oxidizer in sound producing fire crackers, KNO_3 with sulphur, aluminium and boric acid.

Experimental

Chemicals and materials

The chemicals used for the preparation of fire cracker were obtained from a firework manufacturing company situated in Tamilnadu, India. The purity and assay of the chemicals are: KNO_3 – 97.6%, Sulphur (S) – 99.9%, Aluminium (Al) – 99.8% and boric acid (H_3BO_3) – 99%. Aluminium powders were of grade 999 (200 mesh, 75 microns), KNO_3 of 120 mesh and 125 microns, S of 100 mesh and 150 microns and H_3BO_3 of 100 mesh and 150 micron sizes were used. All these chemicals were sieved through a 100 mesh brass sieve. The samples were stored away from light and moisture. All these samples were mixed in the ratio of KNO_3 : Al : S : H_3BO_3 as 57.5/20/22/0.5 %.

Instruments

Thermal analyser

Thermal analysis (TA), thermogravimetric (TG) and differential thermal analysis (DTA) were carried out using a Perkin-Elmer, Pyris diamond

model thermal analyser with a heating rate of 1, 10 and 20 °C min^{-1}, and a temperature range of the standard system of room temperature to 900 °C.

X-Ray diffraction analyser

The pyrotechnic mixture and its intermediate products on decomposition were analysed by X-ray analysis by employing a Siemens 800 X-ray diffractometer (XRD) with Cu Kα radiation with a view to characterising the intermediate products of decomposition. Thermal runs of the pyrotechnic mixture were interrupted in the TGA-DTA system (heating rate 10 K min^{-1}, cooling rate 60 K min^{-1}) and the intermediates in the range of temperatures, 280–300 °C and 950–980 °C were collected and the collected residues were analysed by XRD. Adequate care was taken to avoid moisture pick up before XRD analysis.

Results and discussion

Figure 1 shows the simultaneous TGA, DTG and DTA curves of pyrotechnic mixture obtained at a heating rate of 10 K min^{-1} under N_2 atmosphere. The decomposition patterns obtained under other heating rates are similar and the increase in heating rate leads to an increase in the characteristic peak temperature (T_p) which can be seen in the thermograms (Figure 2).

DTG analysis showed that decomposition occurred in three stages: the first stage ranges from 150 to 250 °C, the second stage is in the range from 580 to 680 °C and the third stage ranges from 750 to 850 °C (Table 1).

Decomposition occurred only in three stages by increasing the heating rate. In TG analysis, the second and third stages are not clearly differentiated. Pyrotechnic mixture before decomposition and residues after the first and third stages of decomposition were collected and were analysed by XRD analysis (Figure 3). Powder diffraction patterns are typically plotted as the intensity of the diffracted X-rays *versus* the angle 2θ. Peaks will appear in the diffraction pattern at 2θ values when constructive interference is at a maximum. By measuring the 2θ values for each diffraction peak, the *d*-spacing (the distance between the diffracting planes) can be calculated automatically by the data analysis software for all of the peaks in the diffraction pattern. The 2θ values obtained from the XRD pattern were compared with standard JCPDS (Joint Committee on Powder Diffraction Standards) data and marked in the XRD pattern in Figures 3–5.

The sharp mass loss at 150–250 °C is assigned to the removal of sulphur making a weight loss of

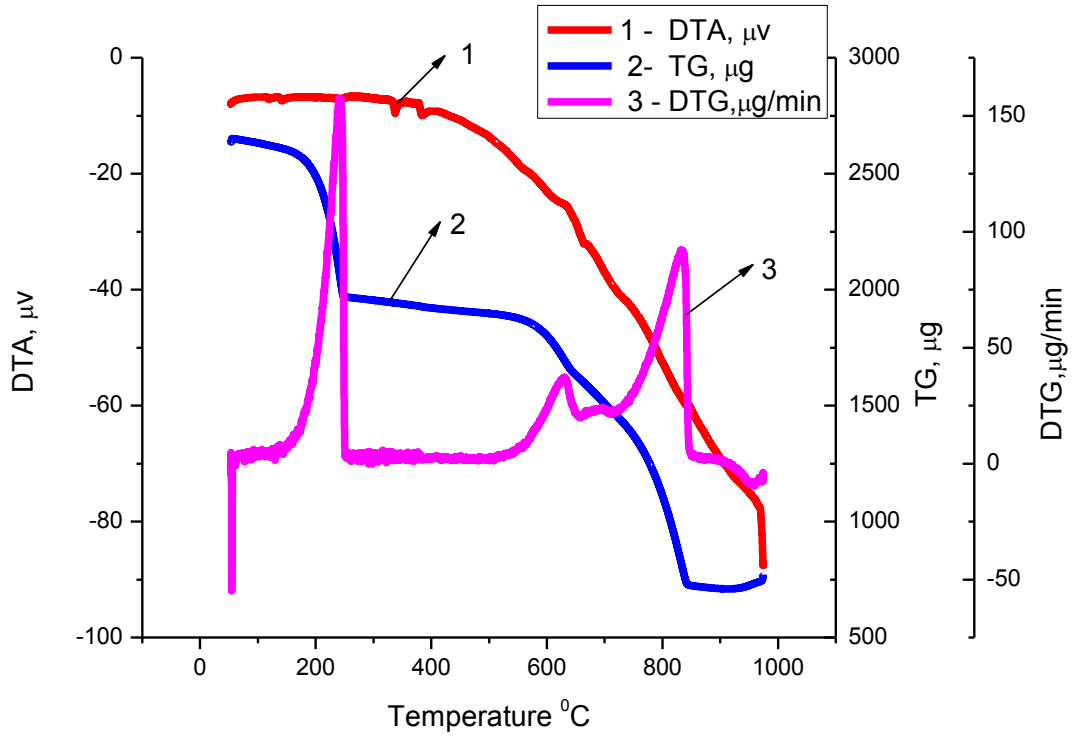

Figure 1. *TG, DTA and DTG curves of $KNO_3/S/Al/H_3BO_3$ in N_2 atmosphere; heating rate: 10 K min^{-1}.*

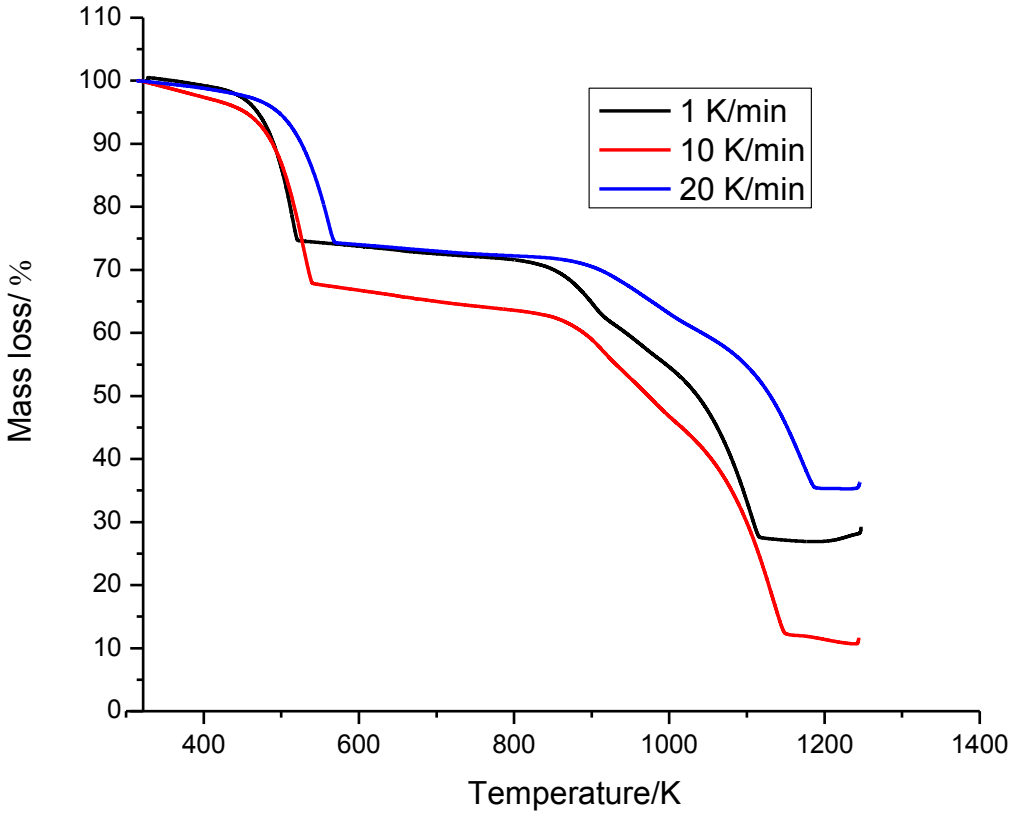

Figure 2. *TG analysis of $KNO_3/S/Al/H_3BO_3$ in N_2 atmosphere; at three different β: 1, 10, 20 K.*

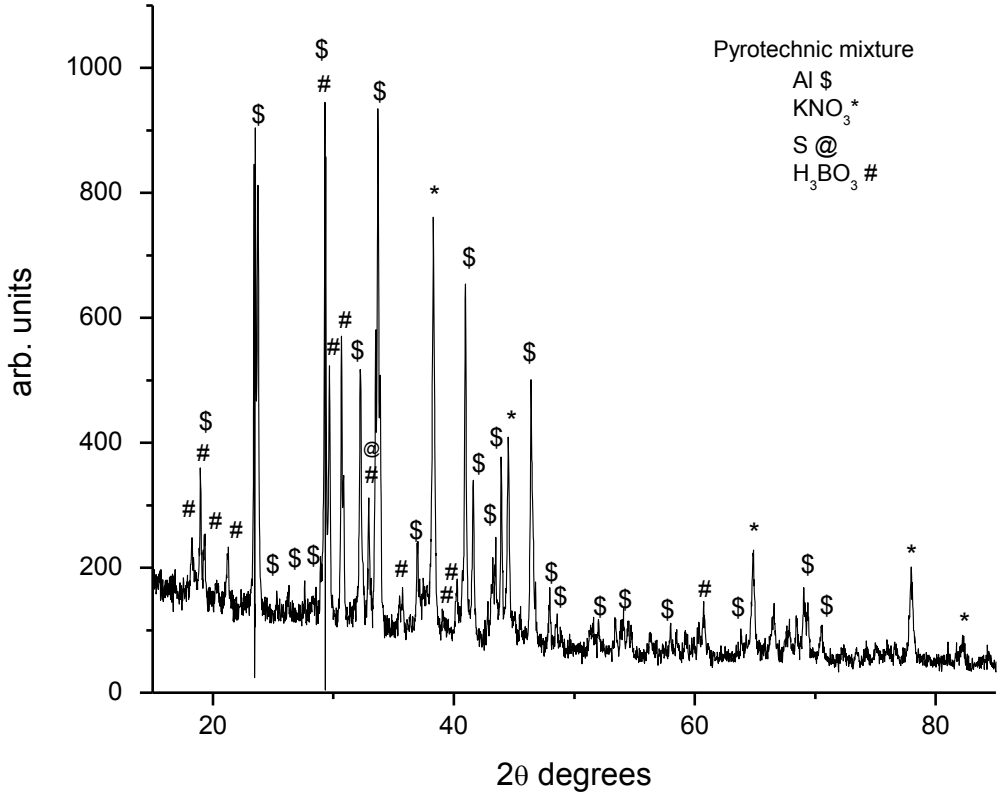

Figure 3. *XRD pattern of pyrotechnic mixture, $KNO_3/S/Al/H_3BO_3$, before decomposition.*

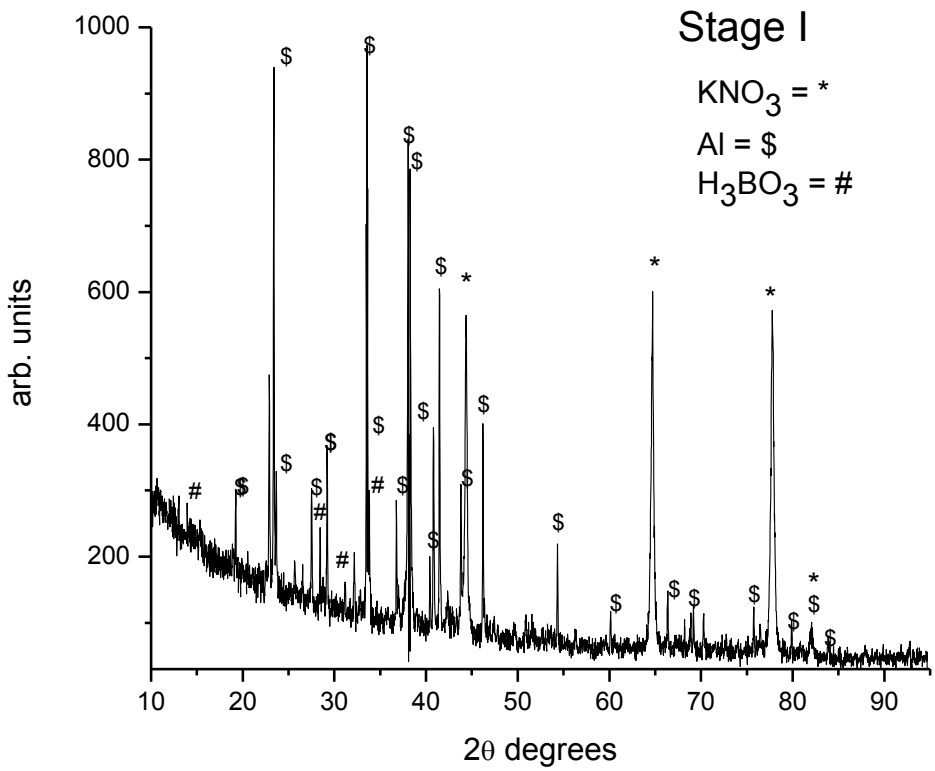

Figure 4. *XRD pattern of the residue after decomposition between 280 and 300 °C.*

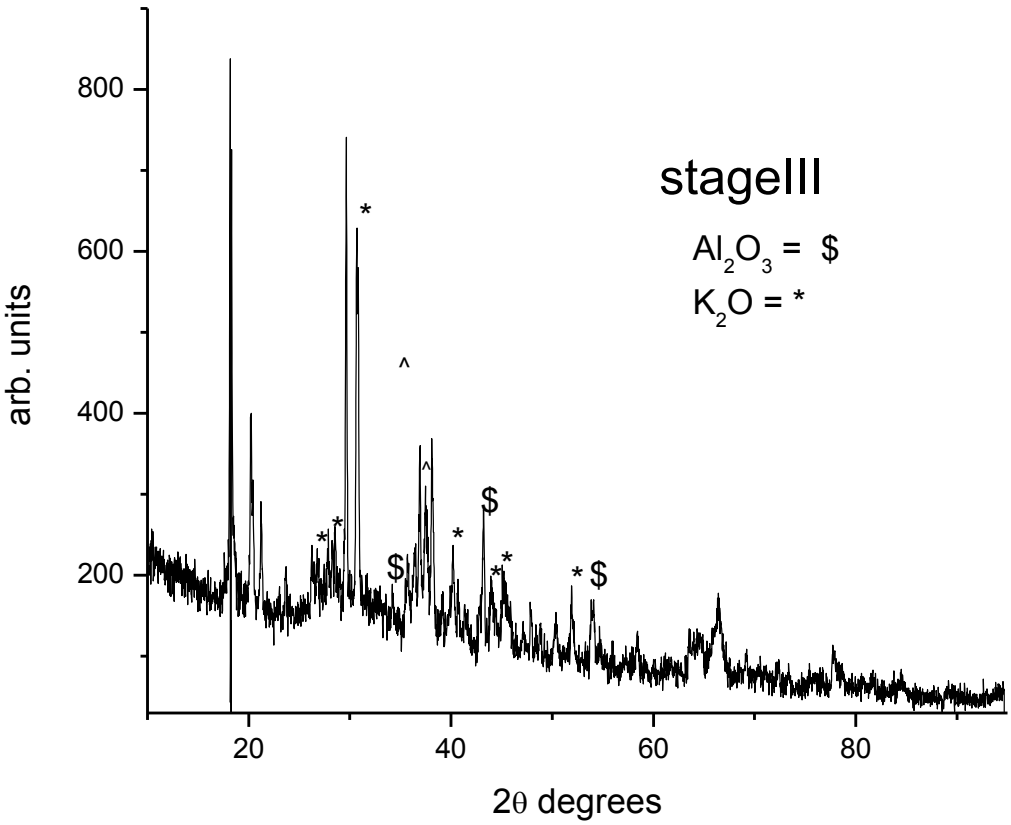

Figure 5. *XRD pattern of the residue after decomposition between 950 and 980 °C.*

Table 1 *Comparison of the expected and the observed mass loss for the decomposition of KNO_3/Al/S/H_3BO_3 at 10 K min^{-1} under nitrogen atmosphere*

Stages	Temperature	Assumed reactions	Weight loss (TG data) (%)	
			Observed	Expected
I	150–250 °C	$S \rightarrow S(l) \rightarrow S(g)$	24	22
II	580–680 °C	$2KNO_3 \rightarrow 2KNO_2 + O_2(g)$	15	15.84
III	750–850 °C	$4Al + 3O_2(g) \rightarrow 2\ Al_2O_3$ $4KNO_2 \rightarrow 2K_2O + 4NO(g) + O_2(g)$	35	35.29

24% by exothermic reaction. The exothermic reaction indicated the conversion of sulphur into molten melt by melting or fusion and is a physical process that results in the phase transition of a substance from a solid to a liquid, at which the ordering of ionic or molecular entities in the solid breaks down to a less ordered state and the solid liquefies. Substances in the molten state generally have reduced viscosity with elevated temperature; an exception is the element sulphur, whose viscosity increases to a point due to polymerization and then decreases with higher temperatures in its molten state. Sulphur is not removed by sublimation which is an endothermic phase transition of a substance directly from the solid phase to the gas phase without passing through an intermediate phase and requires additional energy.

In the fire crackers, it is assumed that all the sulphur taken in the pyrotechnic mixture is converted to sulphur dioxide and the reaction is highly exothermic providing energy to initiate the reaction of the pyrotechnic mixture. The absence of peaks due to sulphur (Figure 4) confirms the removal of sulphur in the first stage as shown in the XRD of the residue at stage I.

The second stage of mass loss which occurred between 580–680 °C is assigned to decomposition of oxidizer, KNO_3, liberating oxygen. Liberation of oxygen from the oxidizer causes 15% weight loss and the reaction is exothermic. The third stage of decomposition occurred immediately after stage II of decomposition between 750–850 °C with 35% mass loss corresponding to the expulsion of NO gas and as the heating rate increases, the temperature difference between these two stages is narrowed down. Complete exothermic reaction of pyrotechnic mixture occurred at stage III leaving only Al_2O_3 and K_2O as residue which were collected for XRD analysis. The XRD pattern (Figure 5) supported the suggested mechanism and confirmed the final residue obtained from the fire cracker is only potassium oxide and aluminium oxide (Table 1).

Based on the observations of weight loss from TG data of pyrotechnic mixture by three stages, the mechanism given in Table 1 is assumed to take place. There is good agreement between the expected theoretical mass loss and the observed mass loss for all the stages of decomposition of pyrotechnic mixture of KNO_3 : Al : S : H_3BO_3 in the ratio of 57.5/20/22/0.5 % shown in Table 1.

The kinetics of the thermal decomposition of sound producing pyrotechnic mixture, KNO_3/S/Al/H_3BO_3 under N_2 atmosphere at different heating rates, were studied by model-dependent and model-free methods for each stage separately.

Determination of energy of activation, E_a: model-free methods

The transformation rate during a reaction is the product of two functions, one depending solely on the temperature, T, and the other depending solely on the fraction transformed, α:

$$d\alpha/dt = f(\alpha).k(T) \qquad (1)$$

where $d\alpha/dt$ is the derivative of the fraction converted with respect to time. It was calculated for every 10% mass loss of the mixture for all

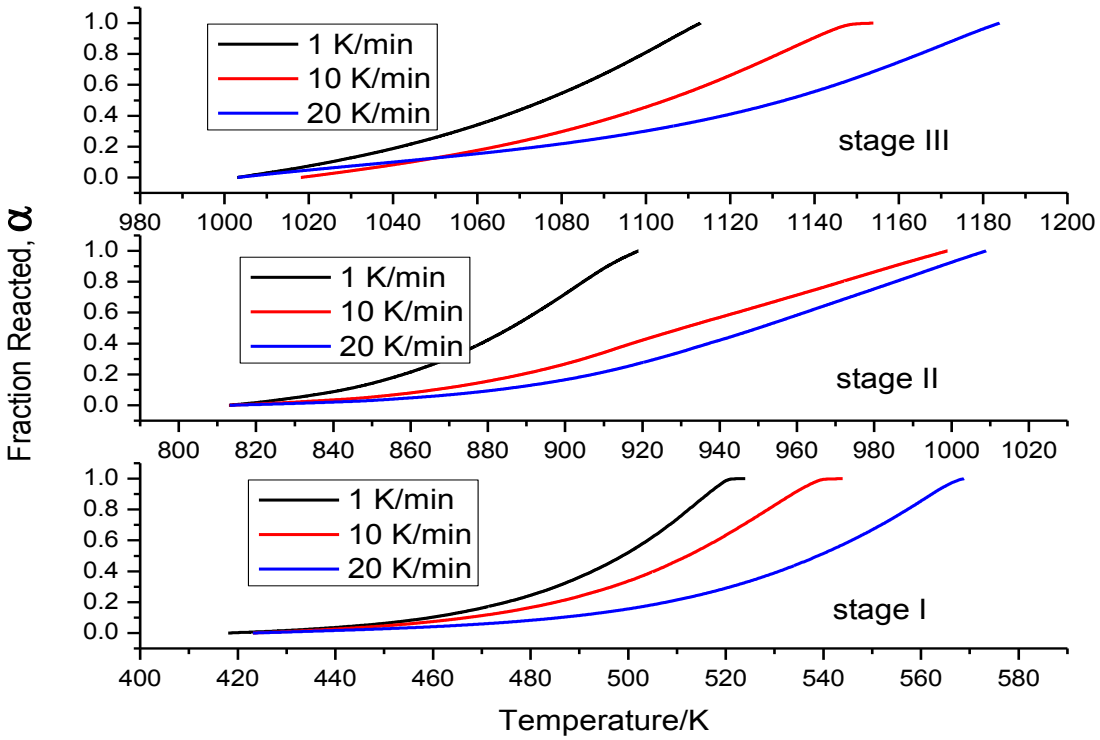

Figure 6. *Fraction reacted, α, versus temperature for stages I, II and III at three different heating rates.*

the three stages of decomposition in the temperature range of 150–250 °C, 580–680 °C and 750–850 °C respectively at different heating rates. α is defined by the expression as

$$\alpha = (\%w_i - \%w_t)/(\%w_i - \%w_f) \quad (2)$$

where $\%w_t$ is the mass percent at any time t and $\%w_i$ and $\%w_f$ are the initial and final mass percent sample,[9–15] respectively. A typical plot of α versus temperature for stages I, II and III is shown in Figure 6.

The temperature dependent function is generally assumed to follow an Arrhenius type[9–13] dependency:

$$\ln k = \ln A - E_a/RT \quad (3)$$

Thus, to describe the progress of the reaction for non-isothermal experiments at all temperatures and for all temperature–time programmes, the reaction rate at all times depends on both $f(\alpha)$ and $k(T)$, and hence the determination of $f(\alpha)$, ln A and E (the so-called kinetic triplet) are needed. The non-isothermal DTG data (Figure 7) were used to calculate the kinetic parameters using Arrhenius method. The linear Arrhenius plots of ln k *versus* $1/T$ for the first stage of decomposition of pyrotechnic mixture at various heating rates were plotted and similar type plots were obtained for other stages also (Figure 8).

From the slope, the activation energy (E_a)[16] for the decomposition of the pyrotechnic mixture was calculated (Table 2). The activation energy values obtained are 30.7 ± 3.4, 58.23 ± 4.2, 58.83 ± 4.6 kJ mol^{-1} for stages I, II and III respectively.

The activation energy for the non-isothermal decomposition of pyrotechnic mixture was also calculated from the TG data using Kissinger expression:[17]

$$\ln (\beta/T_m^2) = \ln [n(1 - \alpha_m)^{n-1}AR/E_a] - E_a/RT_m \quad (4)$$

where β is the heating rate, A is the pre-exponential factor, E_a is the energy of activation, T_m and α_m are the absolute temperature and mass loss at the maximum mass loss rate $(d\alpha/dt)_m$, and R is the gas constant. This method yielded values of 29.9 ± 2.0, 45.1 ± 2.0 and 108.1 ± 2.0 kJ mol^{-1} for stages I, II and III, respectively (Table 2) from the slope of ln (β/T_m^2) as a function of $1/T_m$ at the maximum mass loss rate (Figure 9).

The fraction reacted, α, 0.10–0.9, was also used for the kinetic analysis using the Flynn–Wall method[18] at different heating rates β using the expression:

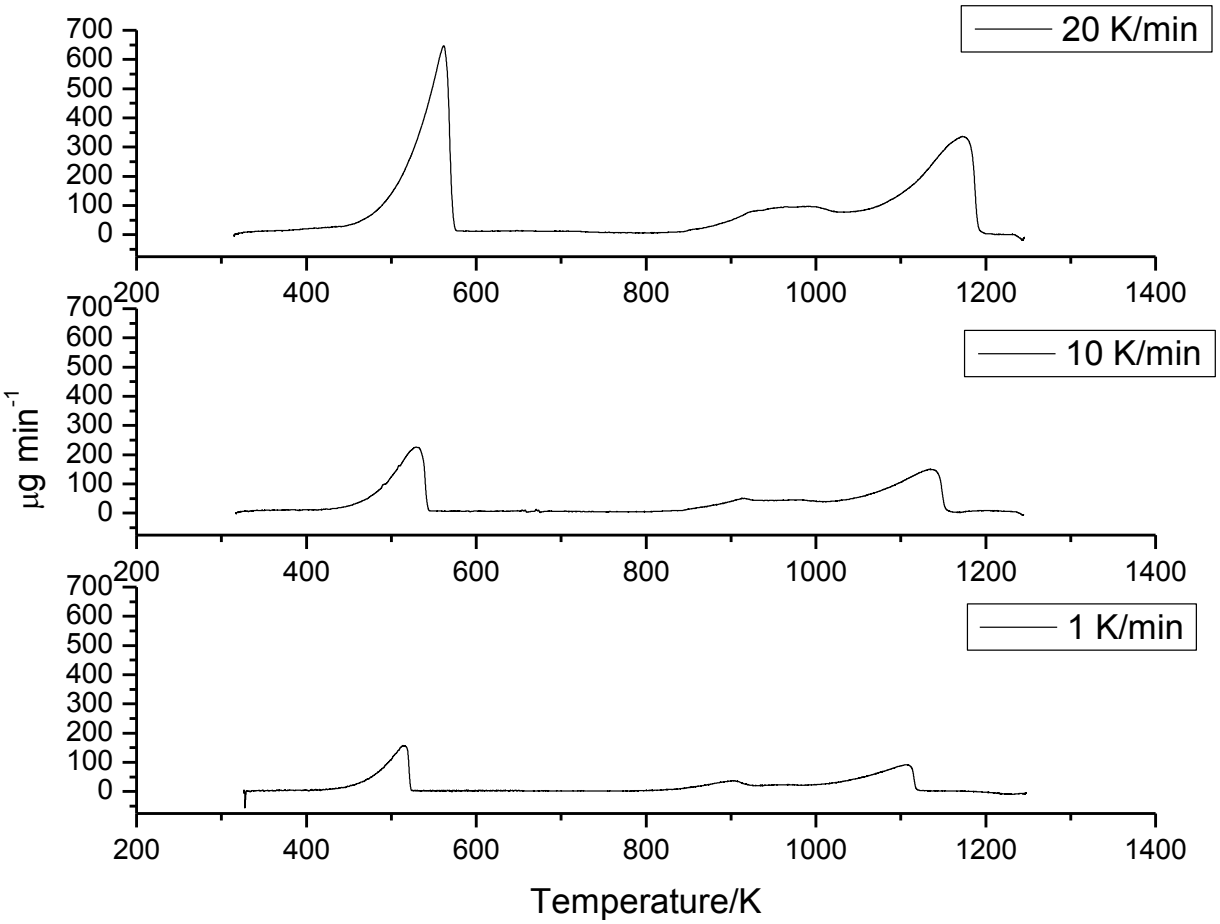

Figure 7. *DTG analysis of KNO_3/S/Al/H_3BO_3 in N_2 atmosphere at three different heating rates.*

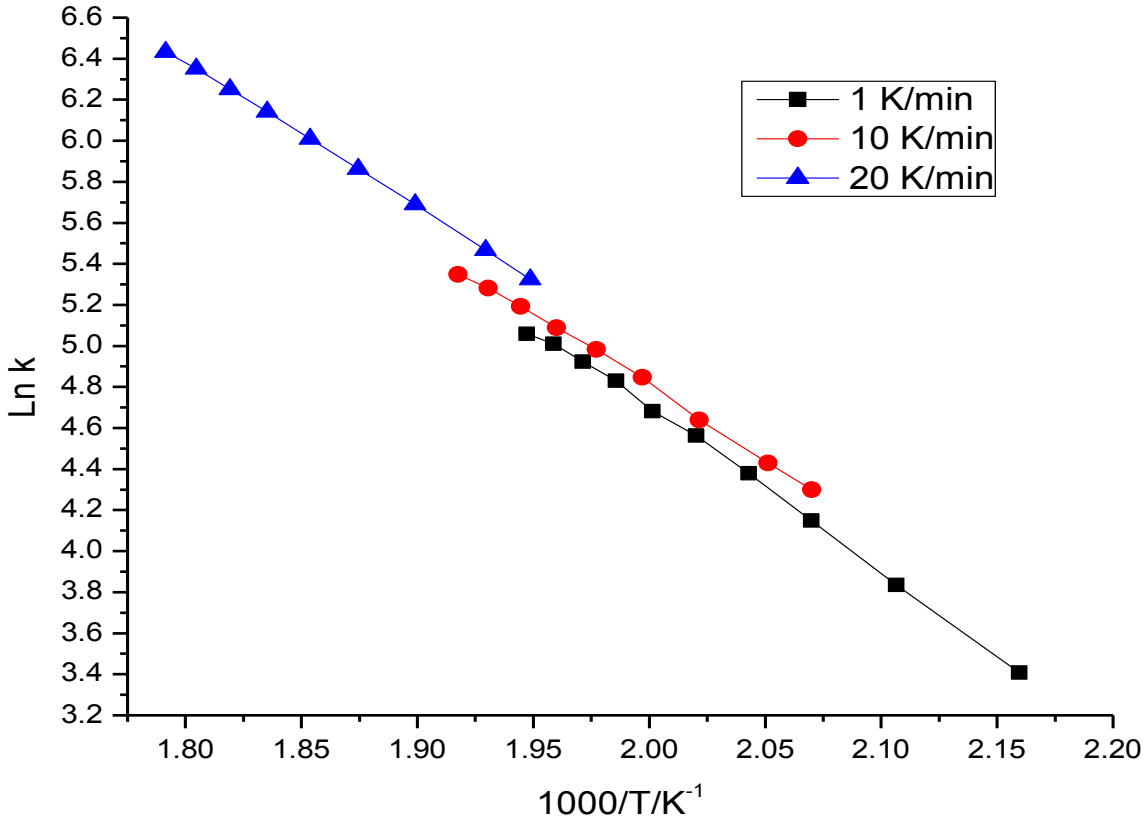

Figure 8. *Arrhenius plot of ln k versus temperature for non-isothermal decomposition of KNO_3/S/Al/ H_3BO_3 in N_2 atmosphere; heating rate: 1,10 and 20 K min^{-1}.*

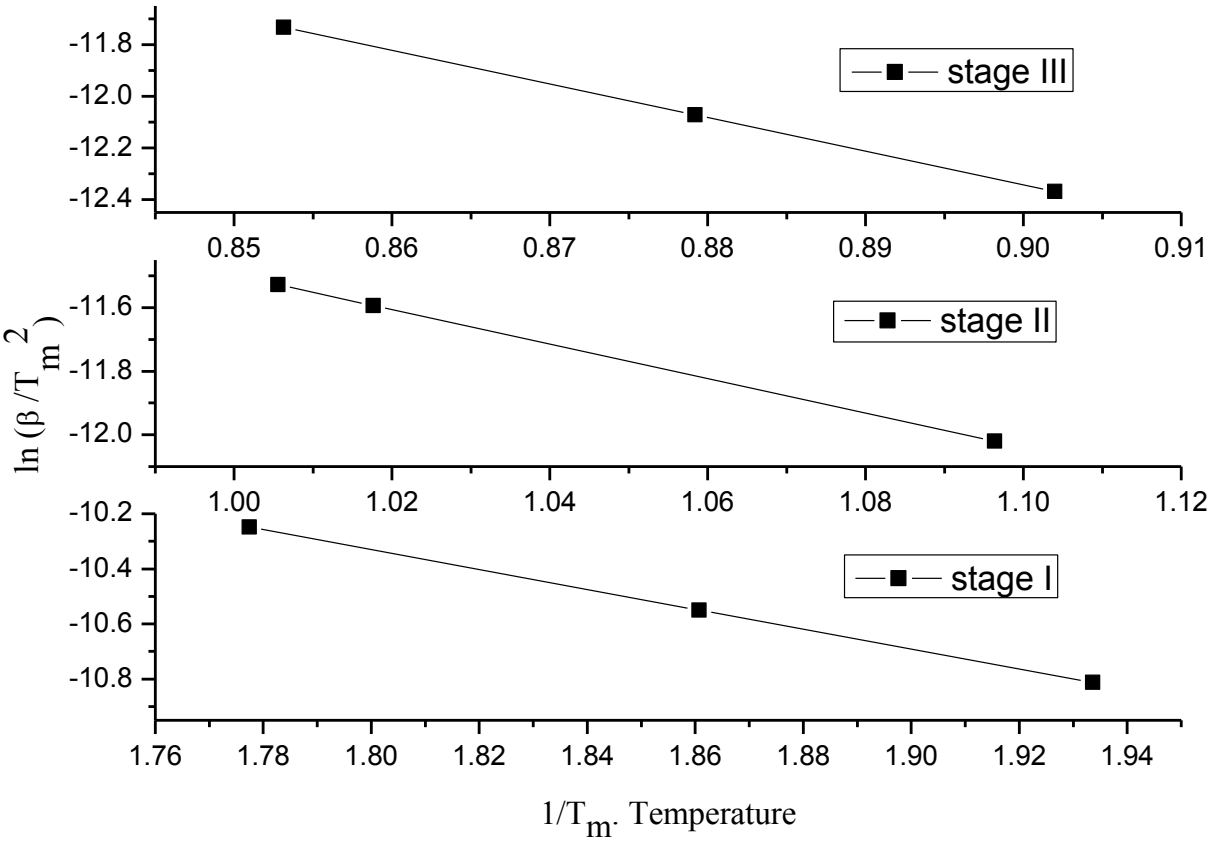

Figure 9. *Kissinger plot for stages I, II and III in N_2 atmosphere for the non-isothermal decomposition of $KNO_3/S/Al/H_3BO_3$ using TG data.*

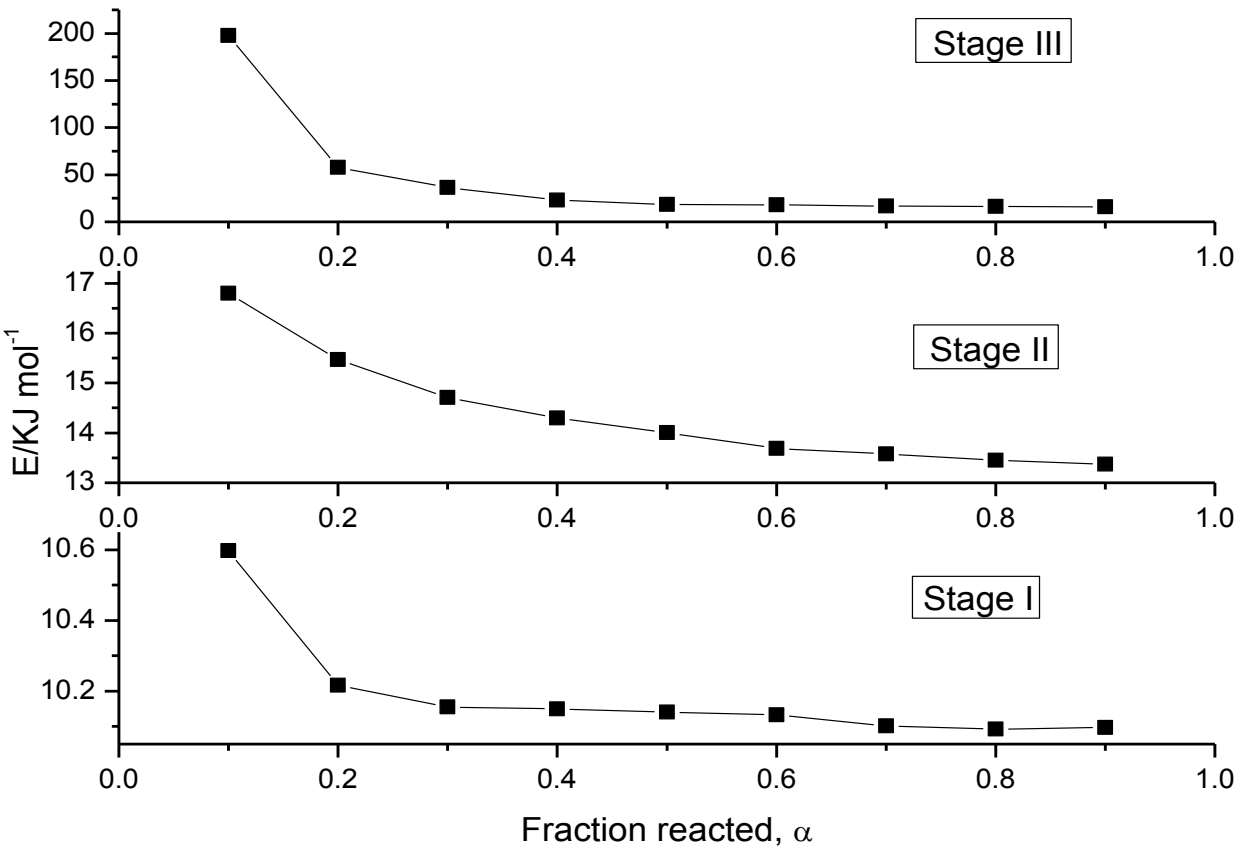

Figure 10. *Apparent activation energy versus α, fraction reacted, for stages I, II and III in N_2 atmosphere for non-isothermal decomposition of $KNO_3/S/Al/H_3BO_3$.*

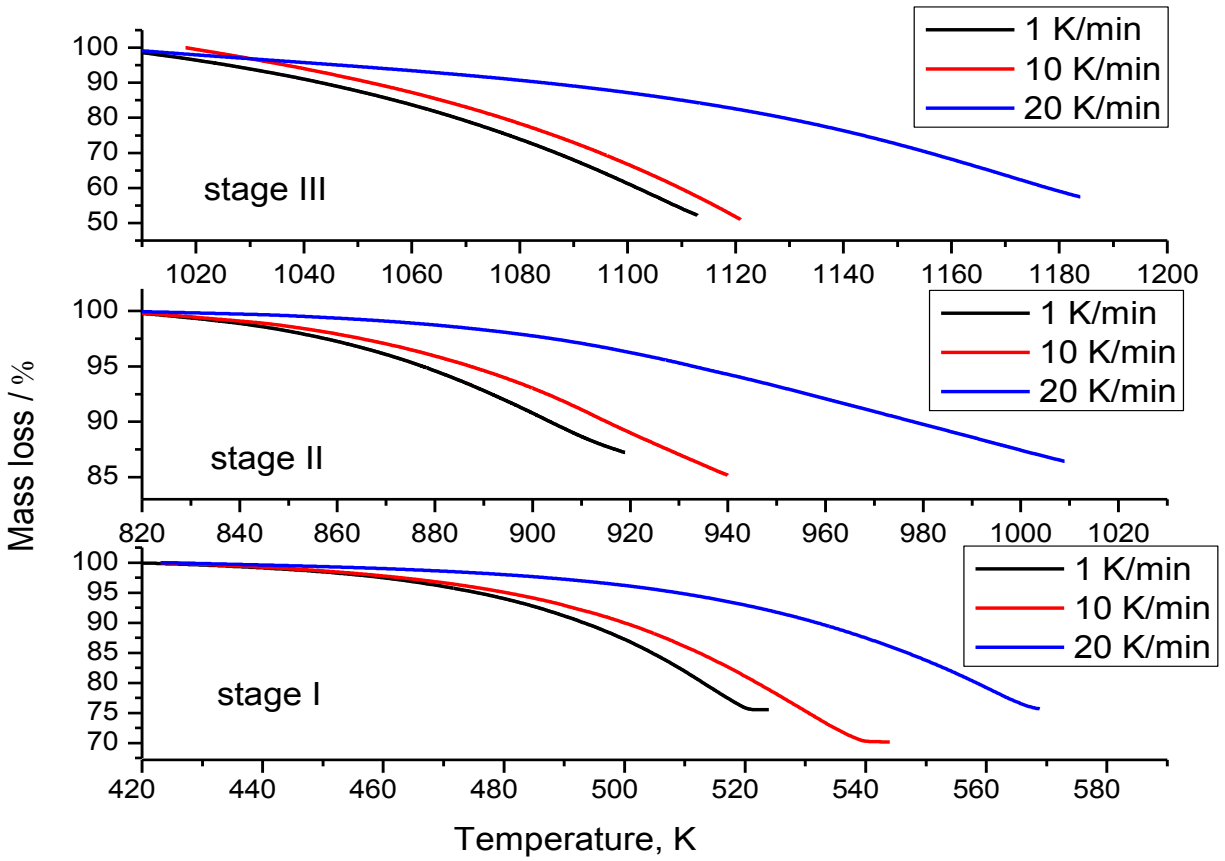

Figure 11. *Mass loss (%) for stages I, II and III versus temperature for the decomposition of KNO_3/S/ Al/H_3BO_3 at different β.*

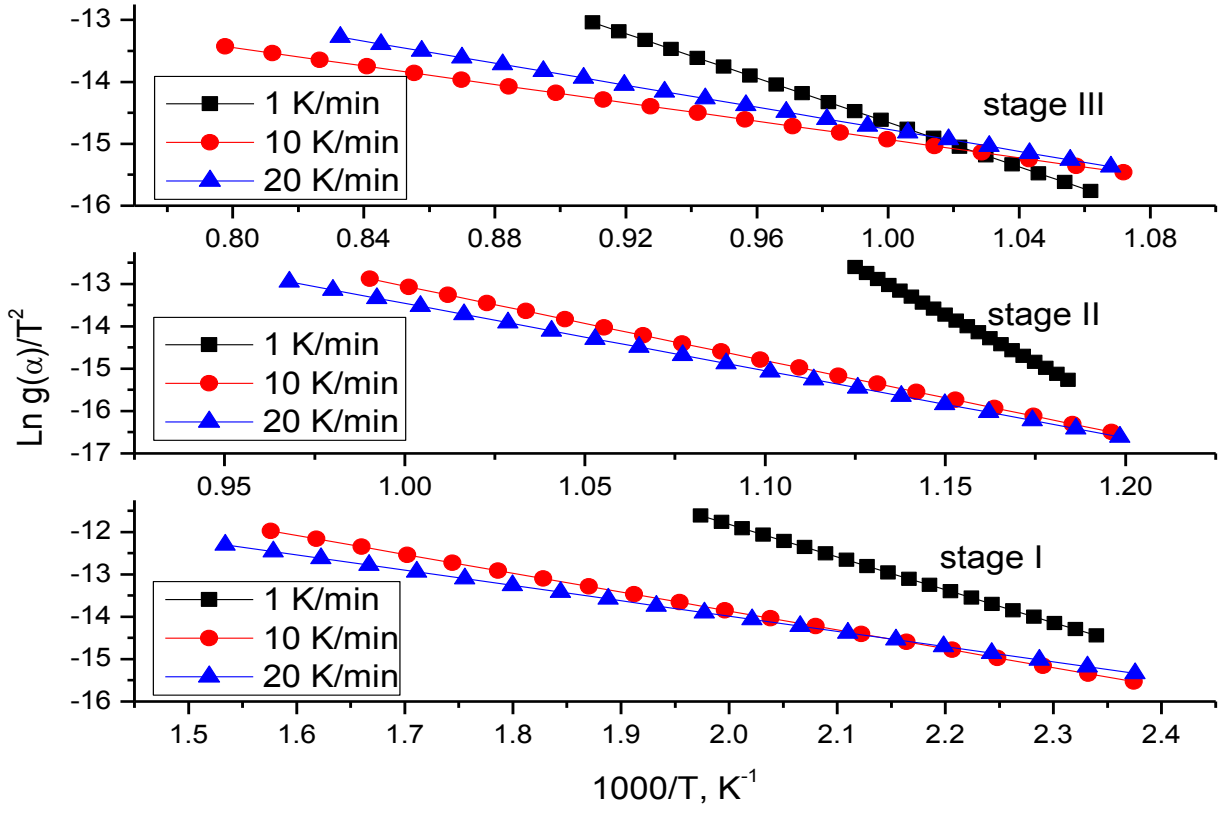

Figure 12. *A2-mechanistic plot of ln g(α)]T^2 versus 1000/T for KNO_3/Al/S/H_3BO_3 in N_2 atmosphere at different β.*

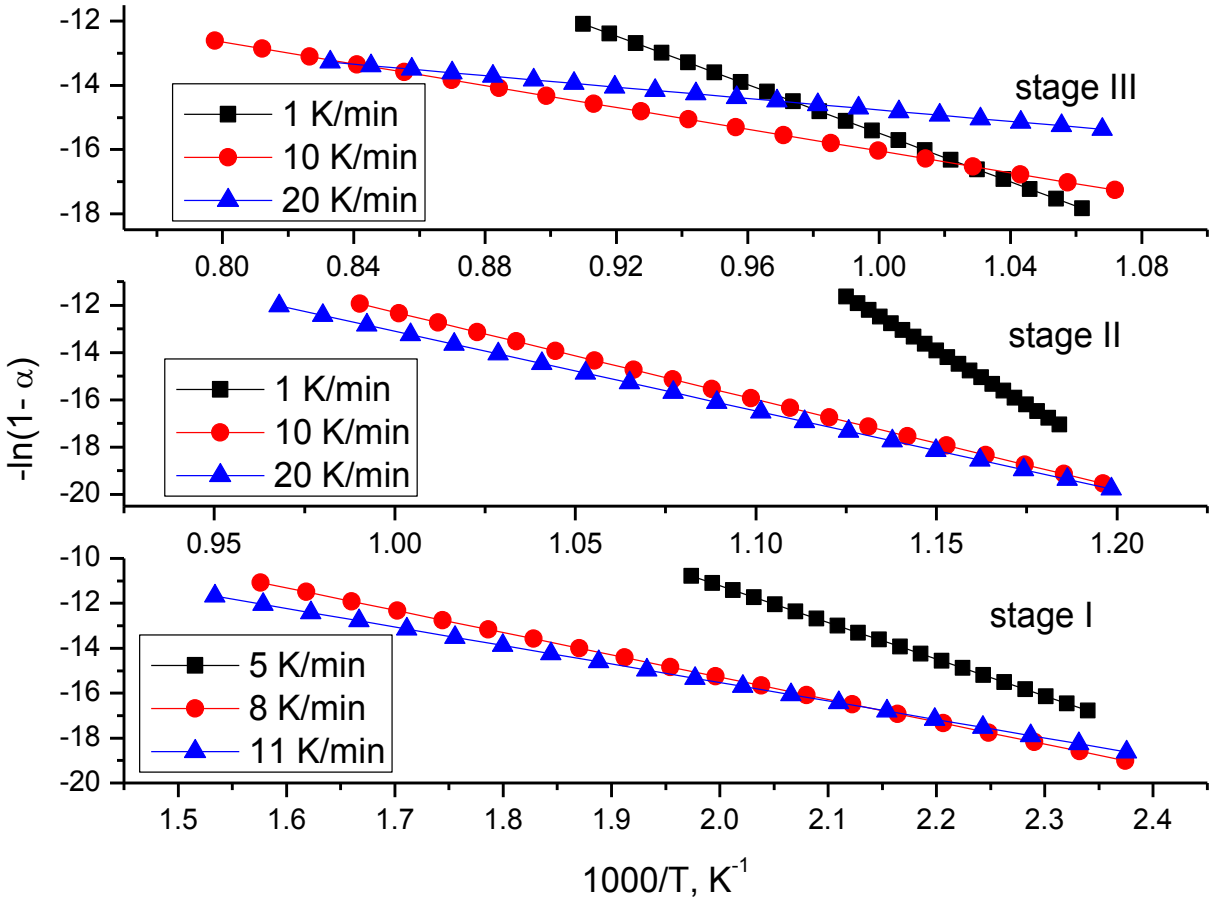

Figure 13. *F1 plot of [−ln(1 − α)] versus 1000/T by KNO_3/Al/S/H_3BO_3 in N_2 atmosphere at different β.*

Table 2 *Activation energy for the decomposition of KNO_3/Al/S/H_3BO_3*

Methods	Stages	E/kJ mol^{-1}	Correlation coefficient (r)
Kissinger	I	29.9 ± 5	−0.96452
	II	45.1 ± 5	−0.97819
	III	106.0 ± 2	−0.98159
Arrhenius	I	30.7 ± 4	−0.89253
	II	58.2 ± 6	−0.92733
	III	58.93 ± 6	−0.9157
iso-conversional	I	10.6 ± 4	−0.95209
	II	17.0 ± 6	−0.82797
	III	60 ± 10	−0.92403

Table 3 *List of solid-state rate equations used in the present study*

Description	Equation
Rate controlling mechanism	$g(\alpha)$
P1 power law	$\alpha^{1/n}$
E1 exponential law	$\ln \alpha$
A2 Avrami–Erofe'ev equation 1 .	$[-\ln(1-\alpha)]^{1/2}$
A3 Avrami–Erofe'ev equation 2	$[-\ln(1-\alpha)]^{1/3}$
A4 Avrami–Erofe'ev equation 3	$[-\ln(1-\alpha)]^{1/4}$
B1 Prout–Tompkins	$\ln[\alpha/(1-\alpha)]$
R2 contracting area	$1-(1-\alpha)^{1/2}$
R3 contracting volume	$1-(1-\alpha)^{1/3}$
D1 one-dimensional diffusion	α^2
D2 two-dimensional diffusion	$(1-\alpha)\ln(1-\alpha)+\alpha$
D3 three-dimensional diffusion, Jander's	$[1-(1-\alpha)^{1/3}]^2$
D4 three-dimensional diffusion, Ginstling Brounshtein	$(1-2\alpha/3)-(1-\alpha)^{2/3}$
F1 first order	$-\ln(1-\alpha)$
F2 second order	$1/(1-\alpha)$
F3 third order	$[1/(1-\alpha)]^2$

$$\ln \beta = \ln (AE_a/R) - \ln [F(\alpha)] - E_a/RT \qquad (5)$$

The activation energy for each conversion point (E_a, α) was calculated from the slope of the linear plot of the Flynn–Wall method at different heating rates β. The plots of E_a *versus* α, fraction reacted for stage I, II, III (Figure 10) show that E_a decreases with the extent of conversion (α), $0.2 < \alpha < 0.9$ and the activation energy is high at the initial fraction reacted which indicates that the decomposed products are in equilibrium with the gaseous reactants. The decreasing of E_a with increasing extent of conversion indicates that porous type solids decomposed more easily. The results reveal that the dependence of apparent activation energy (E_a) on the extent of conversion helps not only to disclose the complexity of a decomposition process, but to identify its kinetic scheme as well.

The E_a value is lower for stage I and II (10.444 and 15.88 kJ mol^{-1}) compared to the E_a value of the third stage of decomposition (50.25 kJ mol^{-1}).

Dissociation mechanism – model-fitting method

Kinetic analysis by model-fitting of the thermal data obtained for all the three stages of decomposition was done in order to arrive at the mechanism of the dissociation processes and to deduce the kinetic parameters. The rate of the reaction under non-isothermal conditions can be expressed by the following relation:

Table 4 *Kinetic parameters and possible rate controlling processes of decomposition of KNO_3/Al/S/ H_3BO_3*

Stage	Mechanism	β/K min^{-1}	TG data		Correlation coefficient (r)
			E/kJ mol^{-1}	ln A/min	
Stage I	A2	1	16.054	3.662	−0.96027
		10	12.771	−4.950	−0.97311
		20	11.916	−6.778	−0.97636
Stage II	A2	1	53.316	38.02	−0.88901
		10	25.884	4.518	−0.92033
		20	24.195	2.423	−0.90682
Stage III	A2	1	56.222	3.253	−0.94685
		10	15.729	−7.516	−0.7897
		20	17.212	5.868	−0.90674

$$d\alpha/dT = K(T)/\beta - f(\alpha) \qquad (6)$$

where α is the fraction reacted at temperature T. $f(\alpha)$ is the conversion function which is dependent on the mechanism of the reaction. β is the rate of heating employed in the experiment and $k(T)$ is the rate constant as a function of temperature. Equation (6) can be represented by its integral form as follows:

$$\ln[g(\alpha)/T^2] = \ln[(AR/\beta E)(1 - 2RT/E)] - E/RT \quad (7)$$

The algebraic expression of the integral $g(\alpha)$ functions that are tested in this work are listed in Table 3. A plot of $\ln g(\alpha)/T^2$ *versus* $1/T$ gives a straight line when the correct $g(\alpha)$ function is used in the equation. The $g(\alpha)$ function describes the mechanism of the reaction. Straight lines with a high correlation coefficient and low standard deviation were selected to represent the possible controlling mechanism. The plot of mass loss for the stages I, II and III with respect to the temperature is given in Figure 11. The fraction reacted, α, was evaluated as a function of temperature.

The kinetics of all the three stages of the thermal decomposition of sound producing pyrotechnic mixture, KNO_3/S/Al/H_3BO_3 in N_2 atmosphere at different heating rates was followed by employing the Coats–Redfern[19] approximation (Table 3) which gives the expression.

A plot of $\ln g(\alpha)/T^2$ *versus* $1/T$ gives a straight line when the correct $g(\alpha)$ function is used in the equation. The $g(\alpha)$ function describes the mechanism of the reaction. Straight lines with high correlation coefficient and low standard deviation were selected to represent the possible controlling mechanism. The corresponding kinetic parameters were then calculated and are shown in Table 4. The model-fitting method is performed in the conversion region where the apparent activation energy is approximately constant and where a single model may fit.

The non-isothermal kinetic data of mixture in the limit of $0.2 < \alpha < 0.9$ are fitted to each of the thirteen reaction models which are indicated in Table 3. The values of activation energy (E_a), pre -exponential factor (ln A) and the coefficient of linear correlation (r) for various kinetic models at three different heating rates are presented in Table 4. The Arrhenius parameters (E_a, ln A) are highly variable, exhibiting a strong dependence on the reaction model chosen. On the other hand, more than one model, namely A2 and A3, gave fairly good coefficients of linear equations. However by comparing the E_a value with the model-free method, the A2 mechanism (Figure 11) was accepted.

The corresponding kinetic parameters were then calculated and are shown in Table 4. The best fit for the first decomposition step of expulsion of sulphur, and the second and third decomposition steps of converting aluminium to alumina are obtained using A2, the two-dimensional Avrami

Table 5 *Kinetic parameters and order for $KNO_3/Al/S/H_3BO_3$*

Stage	Order	β/K min^{-1}	TG data		Correlation coefficient (r)
			E/kJ mol^{-1}	ln A/min	
Stage I	F1	1	24.72276	21.60864	−0.96452
		10	18.25368	4.58985	−0.97819
		20	16.55692	0.9595	−0.98159
Stage II	F1	1	100.05091	91.57722	−0.89253
		10	45.28849	24.68004	−0.92733
		20	41.92852	20.51068	−0.9157
Stage III	F1	1	46.16195	22.35522	−0.95209
		10	25.29485	0.93511	−0.82797
		20	28.22128	4.19184	−0.92403

–Erofe'ev model which corresponds to nucleation and growth mechanism. Similarly, the order of the reaction was also found to obey F1 (Figure 12), a first order reaction and the calculated kinetic parameters are given in Table 5.

Conclusions

Thermal analysis of pyrotechnic mixture, KNO_3/ $Al/S/H_3BO_3$, from sound producing fire crackers was carried out at three different heating rates, 1, 10 and 20 K min^{-1}. The thermal decomposition of the pyrotechnic mixture occurred in three stages. The pathway of the decomposition was predicted by analysing the XRD pattern of the residue at stages I and III as sulphur in the mixture is first decomposed exothermically, and the liberated heat energy is used to initiate further exothermic reactions in the mixture leaving K_2O and Al_2O_3 as final residue. The kinetics of thermal decomposition were studied for all three stages and the energy of activation, E_a, was calculated as 10–30 kJ mol^{-1}, 20–58 kJ mol^{-1} and 56–70 kJ mol^{-1} for stages I, II and III respectively by the model-free methods, Arrhenius, Kissinger and isoconversional methods which are in good agreement with the energy of activation, E_a, calculated as 11–16 kJ mol^{-1}, 24–53 kJ mol^{-1} and 15–56 kJ mol^{-1} for stages I, II and III respectively by the model-fitting method A2, a two-dimensional model, nucleation and growth mechanism. The dependence of effective activation energy on extent of conversion shows that the process is kinetically complex. The order of the reactions obeys first order with the energy of activation, E_a, as 16–24 kJ mol^{-1}, 41–53 kJ mol^{-1} and 25–46 kJ mol^{-1} for stages I, II and III respectively. It is our duty to identity some chemicals which can be added to the pyrotechnic mixture so as to increase the E_a value to prevent autoignition of pyrotechnic mixtures while in storage in the fireworks industry. The calculation of the kinetic factor E_a will help to identify the best composition of pyrotechnic mixture for storage.

Acknowledgements

The authors are highly thankful to 'The Standard Fire Works Pvt. Ltd., Sivakasi' for providing fire crackers with suitable proportions of pyrotechnic mixtures and also to scientists, Dr. S. Murugesan and Mr.S. Shyam Kumar, of IGCAR, Kalpakkam for their help in getting XRD and characterizing the data.

References

1 K. Kosanke and B. Kosanke, 'Pyrotechnic ignition and propagation: A review', in *Pyrotechnic Chemistry*, Vol. 4, Journal of Pyrotechnics, USA, 2004, Ch. IV, pp. 1–10.

2 B. Thomson and A. Wild, 'Factors affecting the rate of burning of a titanium-strontium nitrate based compositions', *Proceedings of Pyrochemical International*, United Kingdom, 1975.

3 S. Sivaprakasam and M. Surianarayanan, 'Interrelation between impact, friction, and thermal energy in a pyrotechnic flash reaction', *Journal of Pyrotechnics*, 2006, Vol. 23, p. 51.

4 *Gazette Notification*, 1999, Noise Standards for Firecrackers, G. S. R 682(E).

5 A. Jeya Rajendran and T. L. Thanulingam, 'Sound level analysis of firecrackers', *Journal of Pyrotechnics,* 2008, Vol. 27, pp. 60–76.

6 T. L. Thanulingam, A. Jeya Rajendran, P. Karlmarx, K. Subramanian and A. Azhagurajan, 'Hazard assessment and effect of nano-sized oxidizer on sound level analysis of firecrackers', *Journal of Pyrotechnics*, 2009, Vol. 28, pp. 95–111.

7 A. Jeya Rajendran and T. L. Thanulingam, 'Effect of particle size and composition of oxidisers on sound level analysis of firecrackers', *Journal of Pyrotechnics*, 2011, Vol. 30, pp. 3–10.

8 M. Fathollahi, S. Pourmortazavi and S. Hosseini, 'The effect of particle size of $KClO_3$ in pyrotechnic compositions', *Combustion and Flame*, 2004, Vol. 138, pp. 304–306.

9 S. Hosseini, S. Pourmortazavi and S. Hajimirsadeghi, 'Thermal decomposition of pyrotechnic mixtures containing sucrose with either potassium chlorate or potassium perchlorate', *Combustion and Flame*, 2005, Vol. 141, pp. 322–326.

10 S. Vyazovkin, A. K. Burnham, J. M. Criado, I. A. Perez-Maqueda, C. Popescu and N. Shirazzuoli, 'ICTAC Kinetics committee recommendations for performing kinetic computations on thermal analysis data', *Thermochimica Acta*, 2011, Vol. 520, pp. 1–19.

11 M. E. Brown, M. Maciejewwski, S. Vyazovkin, R. Nomen, J. Sempere, A. Burnham, J. Opfermann, R. Strey, A. Anderson, R. Kemmler, R. Keuleers, J. Jansens, H. O. Desseyn, C. R. Li, B. Tong, B. Tang, B. Roduit, J. Malek and T. Mitsuhashi, 'Computational aspects of kinetic analysis. Part A: The ICTCA kinetics project data, methods and results', *Thermochimica Acta*, 2000, Vol. 355, pp. 125–143.

12 S. Vyazovkin, 'Kinetic concepts of thermally stimulated reactions in solids, a view from a historical perspective,' International *Reviews in Physical Chemistry*, 2000, Vol. 19, pp. 45–60.

13 S. Vyazovkin, 'On the phenomenon of variable activation energy for condensed phase reactions', *New Journal of Chemistry*, 2000, Vol. 24, pp. 913–917.

14 A. Jeya Rajendran, T. Lekshmana Thanulingam, M. Jose and S. Jerome Das, 'Kinetics and dissociation mechanism of heptaaqua-*p*-nitrophenolatostrontium(II) nitrophenol', *Journal of Thermal Analysis and Calorimetry*, 2011, Vol. 103, pp. 845–851.

15 J. Kitheri, R. Sridharan and T. Gnanasekaran, 'Kinetics of thermal decomposition of $Th(C_2O_4)_2 \cdot 6H_2O$', *Journal of Nuclear Materials*, 2000, Vol. 281, pp. 129–139.

16 M. J. Starink, 'The determination of activation energy from linear heating rate experiments: a comparison of the accuracy of isoconversion methods', *Thermochimica Acta*, 2003, Vol. 404, pp. 163–176.

17 H. E. Kissinger, 'Reaction Kinetics in Differential Thermal Analysis', *Analytical Chemistry*, 1957, Vol. 29, pp. 1702–1706.

18 J. H. Flynn and L. A. Wall, 'A quick, direct method for the determination of activation energy from thermogravimetric data', *Journal of Polymer Science, Part B: Polymer Letters*, 1966, Vol. 4(5), pp. 323–328.

19 A. W. Coats and J. P. Redfern, 'Kinetic parameters from thermogravimetric data', *Journal of Polymer Science, Part B: Polymer Letters*, 1965, Vol. 3, pp. 917–920.

Information for Readers

Editorial Policy

Articles accepted for publication in the *Journal of Pyrotechnics* can be on any technical subject in pyrotechnics. However, a strong preference will be given to articles reporting on research (conducted by professional or serious individual experimenters) and to review articles (either at an advanced or tutorial level). Both long and short articles will be gladly accepted. Also, responsible letters commenting on past Journal articles will be published along with responses by the authors.

Back Issues

Back issues of the Journal will be kept in print permanently as reference material. In addition all past articles and issues are available at the *Journal of Pyrotechnics* - http://archive.jpyro.com.

New Publication Procedures

As announced in Issue 26, the JPyro Board has decided that the Journal will be first published in electronic form and that the hard copy will be published annually. This has been driven by three main factors - the needs of authors to have their papers published in a reasonable timescale, the success of the JPyro archive, and the costs and time required to produce hard copies. In addition the modern publishing and research worlds increasing rely on early electronic publication to provide information to others in the most timely manner and, as appropriate, to be able to claim Intellectual Property rights on material published (which are taken from the date of publication).

In future articles accepted for publication in the Journal will be published, in the first instance, electronically on the JPyro archive website (http://archive.jpyro.com) within a target timescale of three weeks from acceptance (i.e. when all editing is complete) and eight weeks from original submission. All articles will be dated and published in acceptance order. The timescales rely, of course, on referees and authors responding in a reasonable timescale to any queries raised.

In this way no article will be held up awaiting the collation of all the other material necessary for economic and efficient production of the hard copy. Instead, a hard copy of the Journal will be available to those who require it, in most cases annually - incorporating all the articles published within the previous year - for an additional charge. In addition, the JPyro archive will continue to offer online purchase of single articles from the Journal and other publications, or time-limited access to the entire archive.

If you have any questions regarding the new approach please do contact any of the production team

Publication Frequency

Articles in the *Journal of Pyrotechnics* will appear first electronically at http://archive.jpyro.com and will subsequently be produced in hard copy annually in the early spring of the year following publication.

Subscriptions

The following subscription types are available

- Electronic only - access to the electronic versions of articles published during the subscription period indefinitely
- Electronic and Hard copy - as above + hard copy when published
- Single article access - indefinite access to the specified article
- Access to the entire archive - annual access to the full archive

Events and Sponsors

Now that the Journal of Pyrotecnics is published, primarily, electronically the forthcoming events are available on the archive website http://archives.jpyro.com.

If you have any events you would like included in that list please contact the publisher.

Please note

It is our intention in the future to maintain an up-to-date list of current sponsors on the JPyro archive website - http://archives.jpyro.com.

If there are any changes to your details please email sponsors@jpyro.com.

Sponsors of the Journal get unlimted electronic access to the issues which they have sponsored, details online and in the hard copy and a discounted rate for hard copy editions. Please contact the publisher for more details.

Caution

The experimentation with, and the use of, pyrotechnic materials can be dangerous and may require licences or permits in certain countries; it is felt to be important for the reader to be duly cautioned. Without the proper training and experience no one should ever experiment with or use pyrotechnic materials. Also, the amount of information presented in this Journal is not a substitute for necessary training and experience, nor does it remove the relevant application of national or local laws and regulations.

A major effort has been undertaken to review all articles for correctness. However it is possible that errors remain. It is the responsibility of the reader to verify any information herein before applying that information in situations where death, injury or property damage could result.

The Journal of Pyrotechnics Archive

The archive contains downloadable copies of all previous JPyro articles together with copies of other articles published by the Journal of Pyrotechnics. Some of the articles are free to download, but the majority are only available by payment of a per-article fee which will enable perpetual download, or by subscription which will allow access to the entire archive.

The archive will in the future be the primary route to publication. Visit http://archives.jpyro.com